12-2017

3D Seismic Interpretation of a Plio-Pleistocene Mass Transport Deposit in the Deepwater Taranaki Basin of New Zealand

Francisco Jose Rusconi
University of Arkansas, Fayetteville

3D Seismic Interpretation of a Plio-Pleistocene Mass Transport Deposit in the Deepwater Taranaki Basin of New Zealand

A thesis submitted in partial fulfillment
of the requirements for the degree of
Master of Science in Geology

by

Francisco Jose Rusconi
Universidad de Buenos Aires
Bachelor of Science in Geology, 2014

December 2017
University of Arkansas

This thesis is approved for recommendation to the Graduate Council.

_____
Dr. Christopher L. Liner
Thesis Director

_____
Dr. Thomas A. McGilvery
Committee Member

_____
Dr. John B. Shaw
Committee Member

Abstract

A series of Plio-Pleistocene mass transport deposits (MTD) have been identified in the deepwater Taranaki Basin, in New Zealand, using the Romney 3D seismic survey, which covers an area of approximately 2000 km^2. One of these MTDs has been chosen for description and interpretation based on high confidence mapping of its boundary surfaces. The deposit exhibits an array of interesting features similar to those documented by researchers elsewhere plus a unique basal feature unlike those previously observed. The basal shear surface exhibits erosional features such as grooves, "monkey fingers", and glide tracks. Internally, the MTD is typically characterized by low impedance, chaotic, semi-transparent reflectors surrounding isolated coherent packages of seismic facies interpreted as intact blocks rafted within the mass transport complex. Distally, the deposit presents outrunner blocks and pressure ridges.

The new element described in this work consists of a composite feature that includes a protruding obstacle ("shield block") on the paleo-seafloor that acted as a barrier to subsequent flows as they advanced downslope. These blocks disrupt the incoming flow and result in elongate, downflow negative features ("erosional shadow scours"), which are then infilled by the mass transport deposit, and are preserved as elongate isochore thicks.

Kinematic evidence provided by various structures suggests that the MTD flow direction was SE-NW toward bathyal depths. The features presented and the absence of extensional headwall structures, such as local arcuate glide planes and rotated slide blocks, suggest that this part of the deposit belongs to the translational to distal domain of the MTD, and its source area is expected to be somewhere toward the SE in a paleo continental slope.

Acknowledgements

To the University of Arkansas, its faculty and staff for welcoming me and supporting me throughout the program.

To my sponsors: Bec.Ar program for the funding, Fulbright for the administration and LASPAU for the support.

To my advisor, Dr. Chris Liner, for receiving me into his team, for his patience and guidance in this research. To my committee members, Dr. Mac McGilvery and Dr. John Shaw, for their suggestions and comments for this project.

To my friends and classmates, for the great times that I had in Arkansas and field trips. Special thanks to Lanre Aboaba, David Kilcoyne and Andrey Smirnov for sharing the office and creating a good working environment.

To my girlfriend, Mercedes, for her unconditional love and constant support.

To my parents and sister for their education and for allowing me to be where I am today.

Table of Contents

Introduction 1
Geologic Setting 6
Data 8
Methods 9
Results 11
Discussion 20
Conclusions 24
References 27
Figures 34
Appendix 54

Introduction

Mass movements generate the most impressive deposits in terms of volume on the Earth's surface, both in subaerial and submarine environments. Terrestrial deposits may involve up to 10^{10} m^3, whereas submarine mass movements may encompass up to 10^{13} m^3 (Korup, 2012a). The gross depositional process is gravity mass wasting, although there is a wide spectrum of movements such as falls, slumps, slides, flows, and avalanches (Hungr et al., 2001). The mass-transport deposits (MTDs) related to these processes cluster in specific areas such as orogenic belts, fault zones, volcanic arcs, rocky coasts and the edge of continental shelves (Korup, 2012b). Characterization and appraisal of MTD processes and deposits is essential since they not only represent potential natural hazards, but they have also been associated with hydrocarbon traps (Moscardelli et al., 2006; Beaubouef and Abreu, 2010).

Modern MTDs in deepwater settings have been identified using remote data (side-scan sonar, subbottom profiler, reflection seismology) since the second half of the 20th century (Prior et al., 1984). The usage of these techniques plus core and outcrop data, helped to understand morphological and geometrical elements later applied to ancient deposits observed in seismic data. The seismic study of ancient MTDs was originally based on 2D seismic profiles (Weimer and Link, 1991) and interpretation was highly dependent on the interpreter, until the late 1990s when high quality 3D seismic data became more commonly available. Although 3D seismic surveys provided better images, they initially covered relatively small areas compared to the large scale of the deposits. During the 2000s the areal dimensions of 3D seismic surveys were progressively increased facilitating the proliferation of studies on deepwater settings (Shipp et al., 2011).

Principally originating along the shelf/slope break or mid/upper slope in continental margins (with some local smaller exceptions along ridges, mud volcanoes and salt diapirs), MTDs

in deepwater settings lie on the slope and basin floor (Posamentier, 2004; Moscardelli and Wood, 2008), and can represent more than 50% of the near-surface stratigraphic column in these areas (Shipp et al., 2004). Nissen et al. (1999) are the first to document deepwater debris flow features in seismic data in the Nigerian continental slope, reporting outrunner blocks, glide tracks, and pressure ridges, mainly recognized in coherency slices. Currently, MTDs are recognized in seismic data based upon distinct characteristics on their boundary surfaces and internal configuration. It is not uncommon for individual events to amalgamate into a larger composite mass-transport complex. The internal limits between these successive deposits may be hard to recognize in seismic images (Posamentier and Kolla, 2003; Posamentier, 2004; Moscardelli et al., 2006).

MTDs typically exhibit extensional features in the upslope and compressional features in the downslope domains. External geometries may present as sheet, lobate and channel morphologies of variable sizes depending on the flow volumes and degree of fluidization and/or disaggregation. Basal surfaces are characterized by strong seismic amplitude reflectors (Moscardelli and Wood, 2008) and are normally erosional with distinctive scours attributed to the gouging of blocks transported within the flow. These grooves or striations may indicate paleoflow direction as they diverge toward the terminus of the deposit in response to changes in flow conditions ("monkey fingers" in McGilvery and Cook, 2003; "cat-claw scours" in Moscardelli et al., 2006). Internally, the MTDs exhibit chaotic, low-impedance, semitransparent reflection patterns due to the lack of stratification and typically muddy lithology (Posamentier and Kolla, 2003; Shipp et al., 2004). In some cases, coherent packages of seismic facies are observed surrounded by chaotic zones; these are interpreted as intact blocks transported within the flow or undisturbed remnants. In addition, syndepositional thrust faults related to compressional stresses in frontally confined flows can be directed characteristically towards the toe of the deposit. The

upper MTD surface is usually an irregular to hummocky high amplitude reflector, commonly pierced by projected blocks that were transported with the flow (Posamentier, 2004); pressure ridges can appear in distal areas of frontally emergent deposits (Frey-Martínez et al., 2006). Shipp et al. (2004) report that physical characteristics, determined by geotechnical measurements and log responses, suggest that MTDs appear to be more consolidated than equivalent unfailed deposits. Bull et al. (2009) present a detailed analysis of kinematic indicators in MTDs involving the features presented above, and Moscardelli and Wood (2015) establish morphometrical relationships between quantitative parameters (area, length, volume, and thickness) that can be used as predictive tools for areas where MTD exposure or coverage are limited.

There are a variety of MTD triggering mechanisms that include high sedimentation rates, gas-hydrate dissolution, presence of fluids in the sediments, sea-level fluctuations, earthquakes, volcanic eruptions, and storms (Frey-Martínez et al., 2005; Moscardelli et al., 2006). These in turn lead to a number of gravity mass wasting processes involved such as cohesive flow, fluidized flow, and debris flow. The overprinting of different mechanism signatures can make the interpretation of individual processes a challenging task for interpreters. Posamentier and Kolla (2003) interpret the occurrence of MTDs within a sequence stratigraphic progression (from base to top): 1) lower MTD, 2) turbidite frontal-splay deposits, 3) leveed-channel deposits, 4) upper MTD, 5) condensed section deposits. The model suggests that the failure event that produced the underlying MTD also opened a conduit through which the sediments that produced the overlying splay and channel/levee deposit were focused. However, these sequences are mainly attributed to cycles of relative sea-level fluctuations, so it may not appear in areas dominated by other triggering mechanisms.

Several classifications for mass-transport deposits in submarine settings have been proposed in the literature trying to establish some order among this broad term. Most have a

descriptive value and tend to focus on lithology and the processes that generated the deposits (Carter, 1975; Nardin et al., 1979; Ghibaudo, 1992). Recently some interpretative classifications have been proposed. Frey-Martínez et al. (2006) define two end-members for the toe domain that they name "frontally confined" and "frontally emergent". The first exhibits a poor topographic expression and internal large-scale thrust and fold systems, with some preserved stratification. A frontally confined toe involves relatively modest sediment volume and advances by bulldozing the frontal ramp, which determines its distal limit. By contrast, a frontally emergent toe presents major bathymetric expressions (pressure ridges), with core imbricated thrusts, encompassing a larger volume of material that overrides the frontal ramp and travels freely downslope. The authors suggest that these differences are related to the position of the flow center of gravity: under equivalent conditions, frontal confinement is more likely to occur with a lower center of gravity. Moscardelli and Wood (2008) classify MTDs based on their dimensions, causal mechanisms, location of the source area, and relationship of the deposits to the source area, establishing relationships between these four aspects. They initially differentiate regional larger attached MTDs from local smaller ones detached from their source areas. Attached MTDs are further separated based on source area, which is closely related to causal mechanisms: shelf-attached are associated to sea-level fluctuations and high sedimentation rates, whereas slope-attached MTDs are linked to tectonism, volcanism, and storm events, among others. The smaller-scale detached MTDs typically originate from oceanic ridges, mud volcanoes, or salt diapirs due to local instabilities.

Submarine MTDs (principally from the Miocene onwards) have been described in several basins across New Zealand. The earliest work presents data from outcrop (Kuenen, 1950; Ballance, 1964) and refer to these deposits generically as slumps. Gregory (1969) detects folds and thrusts as a tendency of thickening towards the bottom of the slope. Lewis et al. (1980) describe

amalgamated submarine debris-flow deposits commonly lying along sharp erosional surfaces. Collet et al. (2001), in one of the first papers based on seismic data, depicts a modern debris avalanche and an associated debris flow affected by compression due to the subduction of the Pacific Plate beneath the Australian Plate. Since the early 2000s, seismic imaging and areal coverage was improved, chiefly for hydrocarbon exploration in offshore areas and, consequently, studies in MTDs proliferated. Most studies are still based on regional 2D surveys and cover both modern (Joanne et al., 2013; Ogata et al., 2014) and ancient deposits (Lamarche et al., 2008). The most ambitious investigations are those which integrate outcrop, 2D, and 3D seismic data, specifically in the Taranaki Basin's onshore and near offshore. The only study done on mass-transport deposits in the deepwater Taranaki Basin (Omeru et al., 2016) is based in 2D seismic data and mainly focuses on MTD kinematics and extension, but does not include a description of the features that characterize the MTDs.

The current project seeks to identify, characterize and, if possible, catalogue MTDs in the deepwater Taranaki Basin (Figure 1) in order to better understand the geological evolution of the area. The objective is to incorporate and relate elements observed in 3D seismic profiles, time-slices, and horizons for other deepwater ancient MTDs around the world like offshore Nigeria (Nissen et al., 1999), Indonesia and Gulf of Mexico (Posamentier and Kolla, 2003), Brunei (McGilvery et al., 2004), Israel (Frey-Martínez et al., 2005), Trinidad and Venezuela (Moscardelli et al., 2006), and Brazil (Jackson, 2011) that have not been documented in the deepwater Taranaki Basin to date. The main difference with other ancient MTD studies done in the Taranaki Basin (e.g., King et al., 2011; Sharman et al., 2015; Omeru et al., 2016) is that the current work presents elements identified in interpreted 3D seismic horizons. This provides an additional perspective for

the analysis of specific features (scours, blocks, pressure rides) and their characteristics (dimensions, direction, position, relationships) that otherwise would remain unseen.

Geologic Setting

Since most of the Taranaki Basin is submerged, exploration wells and seismic surveys have largely contributed to the knowledge of the region since the 1960s (McBeath, 1977), principally focusing in the onshore and near offshore areas. The basin comprises marine and continental deposits from the mid-Cretaceous to the Cenozoic (Pilaar and Wakefield, 1978; Palmer, 1985; Nodder et al., 1990, King and Trasher, 1992, 1996; King et al., 1993; Vonk et al., 2002; Hansen and Kamp, 2004a, 2006), overlying a pre-Cretaceous basement (Mortimer et al., 1997; Muir et al., 2000; Mortimer, 2004), although modern studies based in seismic 2D profiles and wells logs (Uruski et al., 2003; Uruski and Baille, 2004; Uruski, 2008) consider that the oldest deposits in the deepwater sector are late Jurassic (~160 Ma). Various tectonic settings throughout the basin's history have conditioned its subsidence, depositional environments and structure (Holt and Stern, 1994).

The Taranaki Basin tectonic history and its consequent stratigraphy (Figure 2) can be understood in three different phases according to the plate boundary kinematics since the proto-New Zealand early fragmentation from eastern Gondwana in the late Jurassic until the current configuration (Pilaar and Wakefield, 1978; Knox, 1982; King and Robinson, 1988; King and Trasher, 1996). The basin history was characterized by the initial break-up from Gondwana, followed by a passive margin stage with tectonic calm, and capped by an active margin back-arc basin. The stratigraphy followed in the present research is based on the Romney-1 well technical report (Rad, 2015).

The early basin history starts in the late Jurassic with a pre-rift and break-up phase denoting the differentiation of the proto-New Zealand sub-continent from Australia and East Antarctica, and marking the initial opening of the Tasman Sea. A pre-delta succession and the Taranaki Delta (Uruski, 2008) are the evidence of deposition for this period, which is absent in shallower regions of the basin, with the exception of the Taniwha Formation present in discrete and isolated depocenters throughout the basin and the more widespread Rakopi Formation, equivalent to the uppermost section of the Taranaki Delta. From the Late Cretaceous to the Paleocene a syn-rift to drift stage was settled, spreading the Tasman and developing incipient sub-basins and half-grabens. The deposits in the area related to this setting comprise a series of volcanics and volcaniclastics overlain by the North Cape Formation sandstones and undefined late Cretaceous to Paleocene claystones chronologically equivalent to the lower section of the Turi Formation.

The middle basin history is characterized by a widespread deposition due to a regional subsidence and transgression. From the Paleocene to the Early Oligocene, mostly marine environments were developed in a post-rift to passive margin setting, evidenced by the Eocene calcareous claystones and Oligocene limestones, temporally equivalent to the upper section of the Turi Formation and the Tikorangi Formation, respectively. By the Late Eocene, a transitional tectonic phase began, associated with the progressive influence of the evolving Australian-Pacific plate convergent boundary at the east of the Taranaki basin, although this is only evidenced in some depocenters onshore and shallow offshore.

Establishment of the current active convergent margin during the Early Miocene marked the commencement of the late basin history. Throughout the Miocene, the Taranaki was developed as a foreland basin behind a fold and thrust belt, which in the deepwater area is represented by the distal equivalents of the Wai-iti Group, including a limestone temporally correlatable to the Ariki

Formation marls and outstanding deepwater meandering channels (Li et al., 2017). During the Plio-Pleistocene the current magmatic arc was set, generating a back-arc basin in the Taranaki region. This tectonically active period is embodied in the deepwater region principally by several mass transport complexes, one of which is the subject of the present work.

Data

The primary data set for the present study is a 3D seismic PSTM volume included in the 2016 New Zealand Petroleum Exploration Data Pack, produced by the Ministry of Business, Innovation and Employment of New Zealand. The Romney 3D survey is located in the deepwater Taranaki Basin, approximately 150 km NW offshore from the Taranaki Peninsula on the North Island (Figure 1). The main parameters for this survey and, particularly, the interval of interest are detailed in Table 1.

The Romney-1 well (Table 1) was drilled within the 3D survey. The logs that cover the MTDs interval (seafloor to ca. 2230 m TVD) are gamma ray, caliper and resistivity. Sonic and density logs begin at 2369 m TVD, right below the Miocene reflector, so the generation of a synthetic seismogram for the overlying Plio-Pleistocene MTDs is not possible. Considering this limitation, resolution calculations are done using checkshot data that is available for the whole drilled interval.

Seismic Survey		Well	
Name	Romney 3D	**Name**	Romney-1
Survey type	3D	**Well Type**	Vertical wildcat exploration
Environment	Marine	**Spud date**	26-Nov-2013
Acquisition year	2011	**Completion date**	20-Jan-2014
Area	35x55 km	**Rig type**	Drillship
Bin size	12.5x25 m	**Latitude**	37° 53' 39.337" S
Sample rate	4 ms	**Longitude**	172° 43' 52.719" E
Record length	8.04 s	**Drilling floor**	25 m above sea level
Dominant frequency	41 Hz	**Water depth**	1546.6 m lowest astronomical tide
MTD interval velocity	1850 m/s	**Total depth**	4619 m measured depth
Dominant wavelength	45 m	**Total depth**	4594 m TVD subsea
Vertical resolution	11.25 m	**Result**	Dry hole
Lateral resolution	22.5 m	**Status**	Plugged and abandoned

Table 1. Main parameters for the Romney 3D survey and the Romney-1 well. MTD-D = Mass Transport Deposit of this study. TVD = True Vertical Depth.

Methods

The surveys provided in the data pack are loaded in a Kingdom project, and the interpretation for this research was conducted in Petrel, so the SEGY file for the Romney 3D was exported from Kingdom and imported into Petrel. With the data in Petrel, key horizons were interpreted (Figure 3) to generate time structure maps and observe distinct elements of the MTDs. The MTD analyzed in the present study was chosen (Figure 4) for its widespread extension, and the variety and clarity of its features, and is referred as MTD-D.

Well logs and headers are available as discrete files in the data pack, so those corresponding to the Romney-1 well were directly imported into Petrel, along with checkshots and formation tops included in an Excel summary file. Also using the checkshots, base and top of the MTD-D were provisionally converted from time to depth domain at the borehole.

Resolution calculations were done using checkshots to estimate the MTD interval velocity as 1850 m/s. Frequency values (5–77 Hz) were obtained from spectral analysis for a seismic

volume of a 1-km^2 area around the borehole by 1 second interval below the seafloor (2075–3075 ms) that includes MTD interval studied here. Dominant frequency is 41 Hz, and dominant wavelength approximately 45 m. Therefore, vertical resolution (λ/4) is 11.25 m and theoretical lateral resolution (λ/2) is 22.5 m. Actual lateral resolution is the larger of bin size and theoretical in the inline and crossline directions. For the Romney 3D, the inline bin (NW-SE) dimension is 25 m, so the lateral resolution in that direction is 25 m; the crossline (NE-SW) bin is 12.5 m, so the crossline lateral resolution is 22.5 m.

MTD-D base and top boundary surfaces were converted from time to depth domain. For this, a velocity model was generated using the mentioned surfaces and the well tops previously assigned to these surfaces with the aid of the checkshots. Once the velocity model was generated and the surfaces converted to depth domain, a true vertical thickness (isochore) map was generated to show variations along the survey. For approximate time-depth conversions in this interval, it is considered that 1 ms (two-way time) equals 0.92 m.

The calculation of the MTD-D volume encompassed within the Romney 3D survey was accomplished by applying two different methods. As a first approximation, a basic calculation was done using the area of the survey and the mean of the thickness for the MTD-D isochore in Petrel:

$$Volume = Area \times Thickness \tag{1}$$

$$Volume = (35\ km \times 55\ km) \times 0.08\ km$$

$$Volume = 154\ km^3$$

Due to the irregularity of the boundary surfaces, a more precise calculation was needed to have a better approach to the volume. For that, a 3D grid was created in Petrel using the top and base surfaces converted to depth domain. Having that done, the volume calculation tool was

applied in Petrel for the bulk volume of that grid. The volume obtained through this method in 147.2 km^3.

The error is estimated as:

$$Error = \frac{|Approximate\ Value - Exact\ Value|}{|Exact\ Value|} \times 100\% \quad (2)$$

$$Error = \frac{|154 - 147.2|}{|147.2|} \times 100\%$$

$$Error = 4.6\%$$

Results

An overview of the Romney 3D survey in the deepwater Taranaki Basin allows us to recognize that Plio-Pleistocene MTDs are the most representative deposits for that period of time, and that they comprise an important interval of the stratigraphic column in terms of thickness. As mentioned before, MTD-D was selected among the others to describe and interpret its characteristics. MTD-D has boundary surfaces traceable throughout the whole survey and exhibits a wide variety of high quality features. Unfortunately, the total extent of MTD-D is not covered by the seismic survey, so part of this study addresses what section of the deposit is represented by the Romney 3D survey area.

The mass transport deposit in study is interpreted to be evidence of a debris flow that originated in a paleo continental slope and extends to bathyal depths. In the Romney 3D survey MTD-D covers an area of at least 1925 km^2 and encompasses a volume of 147.2 km^3. It is characterized by a basal shear surface (Figure 5), internal chaotic semi-transparent seismic facies with occasional presence of large intact blocks, and an irregular upper surface (Figure 6). The boundary surfaces are typically high amplitude seismic reflectors. The basal surface is represented

as a high negative amplitude reflector and typically evidences erosive processes. The top boundary of the MTD exhibits a blocky and wavy relief represented by a high positive amplitude hemipelagic condensed-section drape, which is covered by "healing phase deposits" (Posamentier and Allen, 1993) corresponding to turbidites and mud flow deposits. These subhorizontal beds fill to grade local bathymetric irregularities developing progressively more extensive layers as the MTD is completely leveled (Booth et al., 2000; McGilvery and Cook, 2003), evolving into a stable graded slope angle (Prather et al., 1998).

The MTD's distribution is highly conditioned by the bathymetry at the time of deposition: the main portion of the deposit is concentrated at the center of the survey, constrained between bathymetric highs and thins toward the NW (Figure 7). The bulk thickness of the MTD varies from 50 to 100 m, although maximum estimated thickness is 150 m. An additional thick deposit may or may not be related to the main MTD toward the northern corner of the survey. No conspicuous features are displayed in it, and the survey coverage does not establish a clear relationship with the core body, therefore it is not possible to determine if this area represents the same MTD event.

Several distinctive elements can be identified in MTD-D across the survey, defining sectors with unique characteristics and overprinting features. This suggests that the deposit may have been generated in different phases or pulses. A detailed description and interpretation of these elements is presented below.

Coalesced Base

The basal surface of the deposit can be tracked with confidence across most of its extension. It appears as a high negative amplitude reflector more or less continuous throughout the survey. However, toward the most proximal sectors, close to the SE limit of the survey, the presence of a

previous underlying MTD complicates the trace of the basal horizon, defining an area of coalesced base of approximately 400 km^2 (Figure 5).

Mass transport deposits in deepwater settings are commonly draped by hemipelagic condensed sections, represented by high-amplitude positive reflectors (Beaubouef and Friedmann, 2000; Posamentier and Kolla, 2003), but here both stacked deposits were generated sequentially without giving enough time for the drape to develop. Due to the absence of separation between both MTDs, they seem to be fused in this area, making it difficult to distinguish between one deposit and the other one (Figure 8). Mapping was accomplished by tracking discontinuous reflectors with a moderate to high degree of confidence.

Projected Blocks

A prominent feature of the paleo seafloor at the time of MTD-D deposition is the presence of abnormally large blocks. These protruding blocks were transported within the previous mass transport deposits and extend above the average surface elevation of those deposits. These blocks are preserved as local bathymetric highs. The largest blocks are up to 1.5 km wide and 400 m high, and may stand out up to 150 m above the MTD-D base. The projected blocks locally influence the deposition of the subsequent mass transport deposit, which tend to surround and leave these blocks intact. The thickness map reveals that MTD-D is much thinner above the projected blocks relative to the immediate surrounding areas (Figure 7). In the basal surface map (Figure 5), these blocks are identified as discrete bathymetric heights, evidencing that these irregularities were not covered when the MTD-D was deposited. The term "shield block" refers to a new type of feature presented in this study, and is a special kind of projected block.

Shield Blocks - Erosional Shadow Scours

This new type of composite feature introduced in the present study has been documented at least four times in distal areas of the deposit (Figure 9). A shield block consists of an individual protruding block which belongs to an underlying deposit and stands out a certain height at the time of the deposition of MTD-D. The difference with a regular projected block is that the shield block exhibits a downslope elongate negative feature similar to a flute mark, which is later filled by the MTD developing a thicker deposit than in immediate surrounding areas. This local thick includes a cast of the underlying depression. This underlying erosional element is here named as "erosional shadow scour" (ESS), after another contrasting feature described by Moscardelli et al. (2006), which is discussed below. Whether this feature is a real surface element or velocity anomaly artifact is discussed in the Appendix.

As an example, shield block 1 (Figure 9) was deposited by a previous mass transport deposit (MTD-B) and scales up to 1 km wide and 350 m high (Figure 10a). It was projected 140 m above the upper surface of MTD-B by the time of its deposition, assuming that it had not experienced significant erosion until the time it was buried. After that, the shield block was partially covered by subsequent healing phases until the time of deposition of MTD-D, when it still projected ~45 m above the seafloor. The ESS that was generated downslope of shield block 1 is 2.5 km long, 400 m wide, and 30 m deep (Figures 10a, b). The deposit generated within the depression is up to 75 m thick, whereas the contiguous deposit outside the scour is nearly 60 m thick (Figure 10c).

The process behind the formation of such features is as yet not clear. One possibility is development of turbulence downflow of the block as the flow passes around and above it (Figure 11). Subaqueous debris flows are known to travel long distances hydroplaning on a laminar water

cushion (Mohrig et al., 1998, 1999; Elverhøi et al., 2005). Therefore, the flow does not erode the seafloor except for the gauging of large cohesive blocks that become less frequent toward distal areas. When this laminar water cushion encounters an obstacle, it surrounds it and may develop a local downslope turbulence that erodes the substrate. This turbulence persists some distance generating a down system flute-like scour, until the flow returns to its normal laminar behavior. Finally, the flow deposits its bearing sediments in the newly generated scour, where it presents a thicker expression than in laterally equivalent areas.

Curiously, the opposite case has been documented elsewhere. Moscardelli et al. (2006) report mud volcanoes acting as natural physiographic barriers in an MTD in offshore Trinidad. These obstacles develop downslope elongate positive features, that the authors name "erosional shadow remnants" (ESRs), and consist in preserved portions of older seafloor protected from the erosion of passing mass transport flows. This suggests that there might be a difference between the two cases with respect to flow properties and substrate characteristics that determine the generation of either a positive or negative feature. The term applied here is "erosional shadow scour" (ESS).

Internal Body

One of the most distinct characteristics of the main body of MTDs is the presence of cohesive rafted blocks surrounded by a disaggregated matrix. These blocks are identified as coherent packages of seismic facies among chaotic, semi-transparent, low amplitude reflection patterns (Figure 12). The blocks are interpreted as remnants of the failed paleo slope from which the mass transport deposit was originated. Larger blocks are found in proximal areas rather than in distal ones, and some exceed 1 km wide and 200 m high. Occasionally, the blocks cluster

forming larger structures. Both clusters and individual blocks tend to disaggregate progressively with distance and time of transportation towards the toe of the deposit, due to friction with other blocks, the matrix and the seafloor, which is evidenced by completely shattered material in distal areas.

Pressure Ridges

In the western corner of the survey a series of parallel to subparallel arcuate structures seen in the top surface map are interpreted as pressure ridges (Figure 13a). These features form in distal areas of both submarine and subaerial mass transport deposits, are orientated perpendicular to the flow direction, and have the convex side facing downslope (Prior et al., 1984; Posamentier and Kolla, 2003; Bull et al., 2009). In seismic profile, pressure ridges present wavy relief (Figure 14), although internal configuration cannot be seen due to the lack of coherency of the deposit. Applying a variance attribute, higher values can be seen on the flanks of the ridges and lower in the center, evidencing discontinuity between one ridge and the next adjacent feature (Figure 13b). The absence of large cohesive blocks suggests a more disintegrated material, compared to the main body of the MTD.

Prior et al. (1984) attributes the generation of these features to both the interaction of the flow with the seafloor, and the flow's inherent resistance to advance. Laboratory experiments (Marr et al., 2001) have demonstrated that they form when new flows collide with others already resting downslope, implying that the pressure ridges grow through upslope stacking. This is also evidenced in the study area, where distal ridges appear to have a greater degree of erosion than proximal ones, suggesting that they represent an earlier emplacement. Frey-Martínez et al. (2005, 2006) relate the development of pressure ridges to frontally emergent MTDs, where the flow runs

unconfined downslope, in contrast to frontally confined flows which are buttressed against a frontal ramp and usually develop syndepositional thrusts.

Ramps and Flats

Ramps and flats appear as basal features when the flow cuts at different stratigraphic levels (Bull et al., 2009). Flats are bedding-parallel segments of the basal shear surface, whereas ramps are segments of the basal shear surface that cut discordantly across bedding and connect the flat sections. These elements can be identified in the survey toward its southern corner, with an E-W trend. In map view (Figure 15a), the ramps are visualized as sharp downslope linear features that divide areas with topographical differences. In seismic section (Figures 15b, c), they are detected as stratigraphic jumps while tracking the basal surface.

Even though in most cases the ramps are perpendicular to the main flow, there are cases where they are parallel to flow. Therefore, ramps give no kinematic information on their own, and they should be put in context with other features. Some mechanisms have been proposed to explain the development of such elements, although none of them is conclusive. Rupke (1967) has related the differential erosion to localized zones of variable intensity basal shear, whereas Frey-Martínez et al. (2005) suggest that it may be due to mechanical properties of the substrate, the flow, or a combination of both.

Grooves - "Monkey Fingers"

Grooves are identified here as downslope orientated long linear scours, "v" shaped in cross section, which may diverge basinward, following the description by Bull et al. (2009). Starting from the SE limit of the survey, south from the coalesced base, a series of radiating scour features

diverge down system with a W to NW sense. The grooves are easily detected in a basal surface map (Figure 15a), and exhibit a low relief expression of 15 m or less in cross section (Figures 15d, e). These structures have been previously described elsewhere (Posamentier and Kolla, 2003) and named as "monkey fingers" (McGilvery and Cook, 2003) and "cat-claw scours" (Moscardelli et al., 2006) when they exhibit the mentioned divergence. They are associated with large cohesive blocks immersed in the flow that gouge the seafloor during transport and deposition, before lift-off or disaggregation at the termination of the grooves. The occurrence of the divergence is attributed to an abrupt change in the flow conditions due to loss of confinement related to previous bathymetry. Even though the survey does not cover the upward section of the scours where the lines are expected to run confined and parallel, the divergent point seems to be within the survey close to its edge. From this point, lines radiate toward the W for approximately 15 km and the NW for about 20 km, where the gouging blocks were either lifted-off or disaggregated.

Glide Tracks

Unlike the grooves that develop the monkey fingers, glide tracks (Prior et al., 1984; Figure 16) are individual linear features, sometimes slightly to moderately curved, situated in distal areas of the deposit. Excellent examples of such features are located from the center to the NW limit of the survey. The glide tracks are represented by erosional marks in the basal surface map (Figure 17), and the scale can reach 250 m wide, 30 m deep (Figure 18), and 15 km long. The filling of these striations exhibit a thicker sediment expression than the immediate surrounding deposits (Figure 19).

The glide tracks are related to the gouging of outrunner blocks that are expelled down system from the main body of the MTD (Nissen et al., 1999). The uniformity in the scouring of

these features suggest a laminar rather than turbulent flow (Posamentier and Martinsen, 2011). The absence of turbulence allows the scouring blocks to reside at the base of the flow for a prolonged time and develop these long and consistent tracks. Gee et al. (2005) explain that these elongate elements generally lack downslope divergence and are typically flat-bottomed. However, in the study area not only flat-bottomed glides have been found, but also concave ones. This suggests that the relief of the track may depend on the shape of the block and how it interacts with the substrate.

Outrunner Blocks

Previous studies in other areas (Posamentier and Kolla, 2003; McGilvery et al., 2004) have described the lack of preserved blocks that generate glide tracks can be due to either lifted-off or disintegrated downslope. Other studies document the presence of these blocks at the toe of the track, providing information about the sense of transportation (Prior et al., 1984; Nissen et al., 1999; Posamentier, 2004; Moscardelli et al., 2006; Posamentier and Martinsen, 2011). Whether or not the outrunner blocks are preserved depends on the flow conditions and the resistance of the blocks to erosion or disaggregation. In these data, several outrunner blocks are preserved at the end of the glide tracks close to the NW limit of the survey. They are imaged as large isolated coherent clasts down system from the main deposit, and dispersed over the preexisting seafloor (Figure 19). The thickness of the deposits in this area is much thinner than elsewhere, suggesting that these features are located in a distal area of the deposit. It is interpreted that the blocks were projected forward from the main body, although close to the front of the flow, and that immediately after the glide tracks were eroded and the outrunner blocks were emplaced, a depleted flow covered the area. In addition, the area where these blocks are preserved is offset to the north of the axis of

maximum thickness of the MTD (Figure 7), suggesting that there may have been lateral heterogeneities in the flow. The scale of the outrunner blocks (Figure 20) can be as large as 500 m long, 400 m wide, and 100 m high, and its largest axis tends to align with the sense of flow.

The occurrence of outrunner blocks next to the axis of maximum thickness of the MTD suggests lateral nonuniform values of seafloor friction (Minisini et al., 2007). The portion of the flow that expelled outrunner blocks from its front traveled over a rougher base compared to the area of maximum thickness, which slid over a smoother surface (Figures 5, 7). The presence of a rugged bathymetry in the preexisting seafloor due to previous deposits, could have held the advance of the MTD in this area and allowed the forward projection of outrunner blocks. It would be useful to know the thickness of the water cushion on which the flow hydroplaned, and compare that thickness to the bathymetrical variations of the rugged paleo seafloor to determine if these variations could have actually interfered with the bottom of the flow and stopped it. Unfortunately, the possible thicknesses for water cushions or its relationship with the flow's thickness have not been determined.

Discussion

Triggering mechanisms

Several mechanisms have been proposed to explain the causes of submarine MTDs around the world (Moscardelli et al., 2006; Garziglia et al., 2008; King et al., 2011; Lamarche et al., 2016). These triggering mechanisms mostly involve instabilities in the upper continental slope, and usually respond to sea level fluctuations, high sedimentation rates, fluid overpressure, gas hydrate destabilization, and seismicity. Furthermore, these causes have been reported to interact in geologically complex areas (Frey-Martínez et al., 2005).

Based on the 3D survey, there is no apparent cyclicity for the Plio-Pleistocene mass transport deposits in the area, so sea level fluctuations may be discarded as one of the main mechanisms acting here. Conversely, there is evidence of high sedimentation rates up system, starting in the Pliocene (Hansen and Kamp, 2002, 2004b, 2006). The Plio-Pleistocene Giant Foresets Formation documents the rapid southeast-to-northwest progradation of the continental margin in the Taranaki Basin, by migration of fan lobes. These deposits are up to 2200 m thick in some areas of the basin, and were deposited in a period of only 5 Ma (King and Trasher, 1996). This high influx of sediment toward the shelf edge could not only have oversteepened the slope angle but also generated under consolidated deposits, facilitating the development of submarine mass wasting processes.

The Taranaki Basin is known to be the only basin to produce hydrocarbons in the region. The occurrence of gas hydrates and gas migration has been documented in previous works in the area, some of them reaching the present seafloor (Hood et al., 2003; Nyman and Nelson, 2011; Ilg et al., 2012). The releasing of the gas might have increased the pore pressure, reduced the normal stress and the resistance of sediments to flow (Frey-Martínez et al., 2005). Even though gas hydrates may not have acted as triggering mechanisms per se, they could have facilitated the mobilization of large amounts of sediments in the area.

Of all the possible triggering mechanisms, seismicity most commonly mentioned in previous works in the region (Gregory, 1969; Lewis et al., 1980; Collot et al., 2001; Strachan, 2008; Lamarche et al., 2008; King et al., 2011; Omeru et al., 2016), especially for Miocene to Recent MTDs. Since the Early Miocene a convergent margin defines the tectonic setting of the area: the subduction of the Pacific Plate beneath the Australian Plate, with a NW vergence. The Taranaki Basin has experienced active tectonism since the Neogene, first as a foreland basin and

later as a back arc basin. This time interval coincides with the appearance and development of several MTDs in the survey area. The variety in the thicknesses of these deposits and their apparent lack of frequency would suggest that earthquakes played a major role in the slope failures.

Position within the whole deposit

Due to the areal extension of the MTD and limited coverage of the Romney 3D seismic survey, the deposit could not be interpreted over its whole extent. Part of this research is dedicated to analyze to what part of the overall MTD the study area belongs. Although overlap may occur between the different domains, the features presented in the results section can be mainly related to the translational and toe domain (Bull et al., 2009). Ramps and flats, rafted intact blocks, and grooves are typical features present in the translational domain, whereas outrunner blocks with their associated glide tracks, and pressure ridges are more commonly located in the toe domain of MTDs. Because of the lack of knowledge regarding the mechanics that acted on the shield blocks to develop the consequent erosional shadow scours, it is not possible to determine to which domain that element could belong, but it would most likely be part of the two previously mentioned areas. The absence of headwall scarp as well as extensional ridges and blocks suggest that no proximal domain is represented in the survey. According to the morphometric relationships proposed by Moscardelli and Wood (2016), the thickness and the area of the MTD represented in the survey, and the main transportation direction, the source area is estimated to be 10s km southeast from the survey.

Classification

The intention to classify the mass transport deposit interpreted in this study is not for a mere taxonomization, but to take the analysis a step beyond than simply explaining the characteristics of the deposit and the processes that generated it. For this purpose, two interpretative classifications have been chosen.

Frey-Martínez et al. (2006) divide the mass transport deposits into "frontally confined" and "frontally emergent" regarding the characteristics in their toe regions, based on Plio-Pleistocene submarine landslides in the continental margin offshore Israel. The authors suggest that under equivalent conditions, the factor that determines one or the other is the position of the flow's center of gravity: with a lower center of gravity, frontal confinement is more likely to occur. In this case, the studied MTD exhibits several elements that suggest that it could be related to frontally emergent deposits. The prominent bathymetric relief, and the presence of pressure ridges and outrunner blocks indicate that the flow has overridden the frontal ramp and travelled freely downslope. Additionally, the absence of a frontal ramp buttressing the advance of the flow and developing thrusts by bulldozing the foreland supports this idea.

In a classification that focuses on the source areas, although considering the deposit as a whole, Moscardelli and Wood (2008) establish connections between dimensions, causal mechanisms, source area, and relationship of the deposits to their source area. This proposal is based in the analysis of six Plio-Pleistocene MTDs in offshore Trinidad; nonetheless, the authors state that the classification is applicable to other deposits worldwide, providing examples from previous works for each case. They mainly differentiate larger MTDs attached to their source area, either the slope or the shelf edge, from minor detached ones, originated in local submarine bathymetric highs such as mud volcanoes and oceanic ridges. With an area of a few 1000s km^2

and a length of several 10s km, the triggering mechanisms proposed (high sedimentation rates, earthquakes, and fluid pressure in the sediments), and the source area location estimation, the case MTD coincides with the description of attached MTDs. It would require an inspection of the source area, not covered in the survey, to be able to determine if the MTD is attached to the shelf edge or the slope.

Conclusions

The base and top boundary surfaces of a Plio-Pleistocene mass transport deposit (MTD-D) were interpreted throughout the 1925 km^2 Romney 3D seismic survey. This allowed observation and analysis of a wide array of features which illustrate flow processes during the transport and deposition of the sediments.

The volume calculation for the mobilized mass within the Romney 3D survey based on mean interval thickness resulted in an approximate value of 154 km^3 and a computed value that used tracked horizons estimates the volume at 147.2 km^3. A 4.6% difference suggests that the first approximation method would be a reasonable approach for estimating MTD volume. This implies that the mean is a good representation of the interval, and that the irregularities does not signify a major factor in the estimation of the value.

A new composite feature, formed by a shield block and an erosional shadow scour, is introduced here for deepwater mass transport deposits. An erosional shadow scour is associated with a shield block acting as a flow obstacle that develops erosional relief down system. This depression is ultimately filled as a cast by the overlying flow, generating a thicker deposit than the immediate surrounding areas. Although one possible mechanism is proposed in this work, further analysis is needed to fully comprehend the fluid dynamics that can develop these features.

As a first approximation, there seem to be a cocktail of reasons that could explain the development of Plio-Pleistocene MTDs in the basin. Evidence from this research and previous work suggests that several mechanisms could have been operating in the area and finally triggering the flows: high sedimentation rates, gas-hydrate dissolution and pore pressure, and earthquakes. Further research is recommended to determine the proportion and magnitude of each of these processes.

Based on the features observed and documented, it is highly likely that the deposit represented in the survey belongs to the translational and toe domains of a larger MTD. The whole deposit is estimated to be several 10s km long, a few 10s km wide, and cover an area of several 1000 km^2.

Classification of this MTD adds value to seismic interpretation in the area and allows the deposit to be placed in context of other similar MTDs around the world. In addition, this work establishes a pattern of MTD comparison that could be used in future studies in other parts of the deepwater Taranaki Basin. The studied MTD is recognized as frontally emergent and attached to the source area. To determine if the source area is on the shelf or the slope, additional seismic coverage is required 10s km southeast the Romney 3D. Analysis of 2D seismic lines in the area could be used to investigate the source area.

The observation and interpretation of MTD-D in the deepwater Taranaki Basin suggest that the most likely development of the deposit is the following scenario. A large mass of sediment (greater than 150 cubic kilometers) failed from the paleo slope due to destabilization by seismicity, and maybe also influenced by high sedimentation rates and the presence of fluids within the sediments. The mass movement may have started as a cohesive landslide but quickly evolved into a debris flow, traveling over a water cushion and carrying large blocks immersed in an intensely

disaggregated matrix. The flow advanced downslope from SE to NW over a heterogeneous paleo seafloor composed by irregular MTDs and smooth healing phase deposits. Both the non-uniformity of the seafloor and the flow have conditioned the development of areas with different erosional and depositional expressions such as the main blocky core, pressure ridges, glide tracks and outrunner blocks, monkey fingers and erosional shadow scours.

The main blocky core aligns with the axis of maximum thickness of the deposit, and exhibits large translated, and eventually clustered, blocks which become less frequent basinward. In contrast, the pressure ridge area is composed of highly disaggregated material, with no presence of large blocks, which could be interpreted as a different phase of the deposit. The glide tracks and outrunner block area is also considered to be a separate phase from the main deposit due to its different kinematics: this portion of the flow, unlike the central core, was stopped by the higher and more irregular paleo seafloor bathymetry, and expelled the outrunner blocks downflow. This non uniform flow has three separated phases, each with its distinct deposits.

Differences in the flow conditions and the interaction of the flow with the substrate are also evidenced in erosional features. Changes in the bathymetry and the subsequent loss of flow confinement resulted in the divergence of grooves interpreted as monkey fingers. Ramps and flats evidence the unevenness in both the flow and the resistance of the substrate to erosion: in this case, the developed features are aligned with the flow main movement direction. Grooves and glide tracks both exhibit a flat longitudinal profile, suggesting that the blocks that gauged the paleo seafloor were carried by a laminar flow at an approximately constant height within it, and not tumbling over the substrate. The irregular bathymetry, specifically due to large protruding blocks deposited by previous flows, and its interaction with the flow also allowed us to describe the new features, here named shield blocks and erosional shadow scours.

The emplacement of mass transport deposits is an extremely complex process. Its erosional and depositional characteristics depend on source area, triggering mechanisms, development of a laminar water cushion, slope, bathymetry and rugosity of the substrate, and volume and lithology of the mobilized material. This study helped to unveil several of the factors that contributed to the deposition of the Plio-Pleistocene MTD-D in the deepwater Taranaki Basin of New Zealand.

References

Ballance, P. F., 1964. The sedimentology of the Waitemata Group in the Takapuna section, Auckland. *New Zealand Journal of Geology and Geophysics*, *7*(3), 466–499.

Baur, J., Sutherland, R., and Stern, T., 2014. Anomalous passive subsidence of deep-water sedimentary basins: a prearc basin example, southern New Caledonia Trough and Taranaki Basin, New Zealand. *Basin Research*, *26*(2), 242–268.

Beaubouef, R. T., and S. J. Friedmann, 2000. High resolution seismic/sequence stratigraphic framework for the evolution of Pleistocene intra slope basins, western Gulf of Mexico: Depositional models and reservoir analogs. In: Weimer, P. et al. (Eds.), *Deep-water reservoirs of the world*. Gulf Coast Section SEPM 20th Annual Research Conference, pp. 40–60.

Beaubouef, R.T., and Abreu, V., 2010. MTCs of the Brazos-Trinity Slope System: Thoughts on the sequence stratigraphy of MTCs and their possible roles in shaping hydrocarbon traps. In: Mosher, D. C., et al. (Eds.), *Submarine Mass Movements and Their Consequences*. Dordrecht, Springer, Advances in Natural and Technological Hazards Research 28, pp. 475–490.

Booth, J. R., DuVernay III, A. E., Pfeiffer, D. S., and Styzen, M. J., 2000. Sequence stratigraphic framework, depositional models, and stacking patterns of ponded and slope fan systems in the Auger Basin: Central Gulf of Mexico slope. In: Weimer, P. et al. (Eds.), *Deep-water reservoirs of the world*. Gulf Coast Section SEPM 20th Annual Research Conference, pp. 82–103.

Bull, S., Cartwright, J., and Huuse, M., 2009. A review of kinematic indicators from mass-transport complexes using 3D seismic data. *Marine and Petroleum Geology*, *26*(7), 1132–1151.

Carter, R. M., 1975. A discussion and classification of subaqueous mass-transport with particular application to grain-flow, slurry-flow, and fluxoturbidites. *Earth-Science Reviews*, *11*(2), 145–177.

Collot, J. Y., Lewis, K., Lamarche, G., and Lallemand, S., 2001. The giant Ruatoria debris avalanche on the northern Hikurangi margin, New Zealand: Result of oblique seamount subduction. *Journal of Geophysical Research: Solid Earth*, *106*(B9), 19271–19297.

Elverhøi, A., Issler, D., De Blasio, F. V., Ilstad, T., Harbitz, C. B., and Gauer, P., 2005. Emerging insights into the dynamics of submarine debris flows. *Natural Hazards and Earth System Science*, *5*(5), 633–648.

Frey-Martínez, J., Cartwright, J., and Hall, B., 2005. 3D seismic interpretation of slump complexes: examples from the continental margin of Israel. *Basin Research*, *17*(1), 83–108.

Frey-Martínez, J., Cartwright, J., and James, D., 2006. Frontally confined versus frontally emergent submarine landslides: a 3D seismic characterisation. *Marine and Petroleum Geology*, *23*(5), 585–604.

Garziglia, S., Migeon, S., Ducassou, E., Loncke, L., and Mascle, J., 2008. Mass-transport deposits on the Rosetta province (NW Nile deep-sea turbidite system, Egyptian margin): characteristics, distribution, and potential causal processes. *Marine Geology*, *250*(3), 180–198.

Gee, M. J. R., Gawthorpe, R. L., and Friedmann, J. S., 2005. Giant striations at the base of a submarine landslide. *Marine Geology*, *214*(1), 287–294.

Ghibaudo, G., 1992. Subaqueous sediment gravity flow deposits: practical criteria for their field description and classification. *Sedimentology*, *39*(3), 423–454.

Gregory, M. R., 1969. Sedimentary features and penecontemporaneous slumping in the Waitemata Group, Whangaparaoa Peninsula, North Auckland, New Zealand. *New Zealand Journal of Geology and Geophysics*, *12*(1), 248–282.

Hansen, R. J., and Kamp, P. J., 2002. Evolution of the Giant Foresets Formation, northern Taranaki Basin, New Zealand. In: *2002 New Zealand Petroleum Conference Proceedings*, pp. 419–435.

Hansen, R. J., and Kamp, P. J., 2004a. Late Miocene to early Pliocene stratigraphic record in northern Taranaki Basin: condensed sedimentation ahead of Northern Graben extension and progradation of the modern continental margin. *New Zealand Journal of Geology and Geophysics*, *47*(4), 645–662.

Hansen, R. J., and Kamp, P. J., 2004b. Rapid progradation of the Pliocene-Pleistocene continental margin, northern Taranaki Basin, New Zealand, and implications. In: *2004 New Zealand Petroleum Conference Proceedings*, pp. 1–9.

Hansen, R. J., and Kamp, P. J., 2006. Sequence stratigraphy and architectural elements of the Giant Foresets Formation, northern Taranaki Basin, New Zealand. *New Zealand Petroleum Conference proceedings*, pp. 6–10.

Herron, D. A., 2011. *First Steps in Seismic Interpretation*. Society of Exploration Geophysicists (pp. 109–112).

Holt, W. E., and Stern, T. A., 1994. Subduction, platform subsidence, and foreland thrust loading: The late Tertiary development of Taranaki Basin, New Zealand. *Tectonics*, *13*(5), 1068–1092.

Hood, S. D., Nelson, C. S., and Kamp, P. J., 2003. Modification of fracture porosity by multiphase vein mineralization in an Oligocene nontropical carbonate reservoir, Taranaki Basin, New Zealand. *AAPG bulletin*, *87*(10), 1575–1597.

Hungr, O., Evans, S. G., Bovis, M. J., and Hutchinson, J. N., 2001. A review of the classification of landslides of the flow type. *Environmental & Engineering Geoscience*, *7*(3), 221–238.

Ilg, B. R., Hemmings-Sykes, S., Nicol, A., Baur, J., Fohrmann, M., Funnell, R., and Milner, M., 2012. Normal faults and gas migration in an active plate boundary, southern Taranaki Basin, offshore New Zealand. *AAPG bulletin*, *96*(9), 1733–1756.

Jackson, C. A.-L., 2011. Three-dimensional seismic analysis of megaclast deformation within a mass transport deposit; implications for debris flow kinematics. *Geology*, *39*(3), 203–206.

Joanne, C., Lamarche, G., and Collot, J. Y., 2013. Dynamics of giant mass transport in deep submarine environments: the Matakaoa Debris Flow, New Zealand. *Basin Research*, *25*(4), 471–488.

King, P. R., and Robinson, P. H., 1988. An overview of Taranaki region geology, New Zealand. *Energy Exploration & Exploitation*, *6*(3), 213–232.

King, P. R., and Thrasher, G. P. 1992. Post-Eocene development of the Taranaki Basin, New Zealand: convergent overprint of a passive margin. In: Watkins, J.S. et al. (Eds.), *Geology and geophysics of continental margins*. American Association of Petroleum Geologists memoir 53: 93–118.

King, P. R., and Thrasher, G. P., 1996. *Cretaceous-Cenozoic geology and petroleum systems of the Taranaki Basin, New Zealand*. Institute of Geological and Nuclear Sciences monograph 13. 243 pp., 6 enclosures. Lower Hutt, New Zealand: Institute of Geological & Nuclear Sciences Limited.

King, P. R., Ilg, B. R., Arnot, M., Browne, G. H., Strachan, L. J., Crundwell, M., and Helle, K., 2011. Outcrop and seismic examples of mass-transport deposits from a late Miocene deep-water succession, Taranaki Basin, New Zealand. In: Shipp, R. C., et al. (Eds.), *Mass-Transport Deposits in Deepwater Settings*. Society for Sedimentary Geology (SEPM) Special Publication 96, pp. 311–348.

King, P. R., Scott, G. H., and Robinson, P. H., 1993. *Description, correlation and depositional history of Miocene sediments outcropping along North Taranaki coast*. Institute of Geological and Nuclear Sciences monograph 5. 199 pp. Lower Hutt, New Zealand: Institute of Geological & Nuclear Sciences Limited.

Knox, G. J., 1982. Taranaki Basin, structural style and tectonic setting. *New Zealand Journal of Geology and Geophysics*, *25*(2), 125–140.

Korup, O., 2012a. Earth's portfolio of extreme sediment transport events. *Earth-Science Reviews*, *112*(3), 115–125.

Korup, O., 2012b. Landslides in the Earth system. In: Clague, J. J., and Stead, D. (Eds.), *Landslides: Types, Mechanisms and Modeling*. Cambridge University Press, Cambridge, pp. 10–23.

Kuenen, P. H., 1950. Slump structures in the Waitemata Beds around Auckland. *Transactions of the Royal Society of New Zealand* (78), 467–475.

Lamarche, G., Joanne, C., and Collot, J. Y., 2008. Successive, large mass- transport deposits in the south Kermadec fore- arc basin, New Zealand: The Matakaoa Submarine Instability Complex. *Geochemistry, Geophysics, Geosystems*, *9*(4), Q04001.

Lamarche, G., Mountjoy, J., Bull, S., Hubble, T., Krastel, S., Lane, E., Micallef, A., Moscardelli, L., Mueller, C., Pecher, I., and Woelz, S., 2016. Submarine Mass Movements and Their Consequences: Progress and Challenges. In: Lamarche et al. (Eds.), *Submarine Mass Movements and Their Consequences*. Springer, Advances in Natural and Technological Hazards Research 41, pp. 1–12.

Lewis, D. W., Laird, M. G., and Powell, R. D., 1980. Debris flow deposits of early Miocene age, Deadman stream, Marlborough, New Zealand. *Sedimentary Geology*, *27*(2), 83–118.

Li, Q., Yu, S., Wu, W., Tong, L., and Kang, H., 2017. Detection of a deep-water channel in 3D seismic data using the sweetness attribute and seismic geomorphology: a case study from the Taranaki Basin, New Zealand. *New Zealand Journal of Geology and Geophysics*, 1–10.

Liner, C. L., 2016. *Elements of 3D Seismology*. Society of Exploration Geophysicists (p. 24).

Marr, J. G., Harff, P. A., Shanmugam, G., and Parker, G., 2001. Experiments on subaqueous sandy gravity flows: the role of clay and water content in flow dynamics and depositional structures. *Geological Society of America Bulletin*, *113*(11), 1377–1386.

McBeath, D. M., 1977. Gas-condensate fields of the Taranaki basin, New Zealand. *New Zealand Journal of Geology and Geophysics*, *20*(1), 99–127.

McGilvery, T. A., and Cook, D. L., 2003. The influence of local gradients on accommodation space and linked depositional elements across a stepped slope profile, offshore Brunei. In: Roberts, H. H. et al. (Eds.), *Shelf margin deltas and linked down slope petroleum systems: Global significance and future exploration potential*. Gulf Coast Section SEPM 23rd Annual Research Conference, pp. 387–419.

McGilvery, T. A., Haddad, G., and Cook, D. L., 2004. Seafloor and shallow subsurface examples of mass transport complexes, offshore Brunei. In *Offshore Technology Conference*. Offshore Technology Conference.

Mohrig, D., Ellis, C., Parker, G., Whipple, K. X., and Hondzo, M., 1998. Hydroplaning of subaqueous debris flows. *Geological Society of America Bulletin*, *110*(3), 387–394.

Mohrig, D., Elverhøi, A., and Parker, G., 1999. Experiments on the relative mobility of muddy subaqueous and subaerial debris flows, and their capacity to remobilize antecedent deposits. *Marine Geology*, *154*(1), 117–129.

Mortimer, N., 2004. New Zealand's Geological Foundations. *Gondwana Research 7*(1), 261–272.

Mortimer, N., Tulloch, A. J., and Ireland, T. R., 1997. Basement geology of Taranaki and Wanganui Basins, New Zealand. *New Zealand Journal of Geology and Geophysics*, *40*(2), 223–236.

Moscardelli, L., and Wood, L., 2008. New classification system for mass transport complexes in offshore Trinidad. *Basin Research*, *20*(1), 73–98.

Moscardelli, L., and Wood, L., 2016. Morphometry of mass-transport deposits as a predictive tool. *Bulletin Geological Society of America 128*(1–2), 47–80.

Moscardelli, L., Wood, L., and Mann, P., 2006. Mass-transport complexes and associated processes in the offshore area of Trinidad and Venezuela. *AAPG bulletin*, *90*(7), 1059–1088.

Muir, R. J., Bradshaw, J. D., Weaver, S. D., and Laird, M. G., 2000. The influence of basement structure on the evolution of the Taranaki Basin, New Zealand. *Journal of the Geological Society*, *157*(6), 1179–1185.

Nardin, T. R., Hein, F. J., Gorsline, D. S., and Edwards, B. D., 1979. A review of mass movement processes, sediment, and acoustic characteristics and contrasts in slope and base-of-slope systems versus canyon-fan-basin floor systems. In: Doyle, L. J., and Pilkey, O. H., (Eds.), *Geology of Continental Slopes*. Society of Economic Paleontologists and Mineralogists (SEPM), Special Publication 27, pp 61–73.

Nissen, S. E., Haskell, N. L., Steiner, C. T., and Coterill, K. L., 1999. Debris flow outrunner blocks, glide tracks, and pressure ridges identified on the Nigerian continental slope using 3-D seismic coherency. *The Leading Edge*, *18*(5), 595–599.

Nodder, S. D., Nelson, C. S., and Kamp, P. J., 1990. Middle Miocene formational stratigraphy (Mokau-Mohakatino Groups) at Waikawau, northeastern Taranaki Basin margin, New Zealand. *New Zealand Journal of Geology and Geophysics*, *33*(4), 585–598.

Nyman, S. L., and Nelson, C. S., 2011. The place of tubular concretions in hydrocarbon cold seep systems: Late Miocene Urenui Formation, Taranaki Basin, New Zealand. *AAPG bulletin*, *95*(9), 1495–1524.

Ogata, K., Mountjoy, J. J., Pini, G. A., Festa, A., and Tinterri, R., 2014. Shear zone liquefaction in mass transport deposit emplacement: a multi-scale integration of seismic reflection and outcrop data. *Marine Geology*, *356*, 50–64.

Omeru, T., Cartwright, J. A., and Bull, S., 2016. Kinematics of submarine slope failures in the deepwater Taranaki Basin, New Zealand. In: Lamarche, G. et al. (Eds.), *Submarine Mass Movements and their Consequences*. Advances in Natural and Technological Hazards Research, vol 41. Springer International Publishing, pp. 61–70.

Palmer, J., 1985. Pre-Miocene lithostratigraphy of Taranaki Basin, New Zealand. *New Zealand Journal of Geology and Geophysics*, *28*(2), 197–216.

Pilaar, W. F. H., and Wakefield, L. L., 1978. Structural and stratigraphic evolution of the Taranaki Basin, offshore North Island, New Zealand. *The APEA Journal*, *18*(1), 93–101.

Posamentier, H. W., 2004. Stratigraphy and Geomorphology of Deep-Water Mass Transport Complexes Based on 3D Seismic Data: Offshore Technology Conference. *Houston, Texas*.

Posamentier, H. W., and Allen, G. P., 1993. Variability of the sequence stratigraphic model: effects of local basin factors. *Sedimentary Geology*, *86*(1-2), 91–109.

Posamentier, H. W., and Kolla, V., 2003. Seismic geomorphology and stratigraphy of depositional elements in deep-water settings. *Journal of Sedimentary Research*, *73*(3), 367–388.

Posamentier, H. W., and Martinsen, O. J., 2011. The character and genesis of submarine mass-transport deposits: insights from outcrop and 3D seismic data. In: Shipp, R. C., et al. (Eds.), *Mass-Transport Deposits in Deepwater Settings.* Society for Sedimentary Geology (SEPM) Special Publication 96, pp. 7–38.

Prather, B. E., Booth, J. R., Steffens, G. S., and Craig, P. A., 1998. Classification, lithologic calibration, and stratigraphic succession of seismic facies of intraslope basins, deep-water Gulf of Mexico. *AAPG bulletin*, *82*(5), 701–728.

Prior, D. B., Bornhold, B., and Johns, M. W., 1984. Depositional characteristics of a submarine debris flow. *The Journal of Geology*, *92*(6), 707–727.

Rad, F., 2015. *PEP 38451 Romney-1 Well Completion Report*. Anadarko New Zealand Taranaki Company for NZP&M, Ministry of Business, Innovation & Employment (MBIE), New Zealand Unpublished Petroleum Report PR4951.

Rupke, N. A., 1976. Large-scale slumping in a flysch basin, southwestern Pyrenees. *Journal of the Geological Society*, *132*(2), 121–130.

Sharman, G. R., Graham, S. A., Masalimova, L. U., Shumaker, L. E., and King, P. R., 2015. Spatial patterns of deformation and paleoslope estimation within the marginal and central portions of a basin-floor mass-transport deposit, Taranaki Basin, New Zealand. *Geosphere*, *11*(2), 266–306.

Sheriff, R. E., 2002. *Encyclopedic Dictionary of Applied Geophysics*. Society of Exploration Geophysicists (p. 380).

Shipp, R. C., Nott, J. A., and Newlin, J. A., 2004. Physical characteristics and impact of mass transport complexes on deepwater jetted conductors and suction anchor piles. In *Offshore Technology Conference*. Offshore Technology Conference.

Shipp, R. C., Weimer, P., and Posamentier, H. W., 2011. Mass-transport deposits in deepwater settings: an introduction. In: Shipp, R. C., et al. (Eds.), *Mass-Transport Deposits in Deepwater Settings*. Society for Sedimentary Geology (SEPM) Special Publication 96, pp. 3–6.

Strachan, L. J., 2008. Flow transformations in slumps: a case study from the Waitemata Basin, New Zealand. *Sedimentology*, *55*(5), 1311–1332.

Uruski, C., 2008. Deepwater Taranaki, New Zealand: structural development and petroleum potential. *Exploration Geophysics*, *39*(2), 94–107.

Uruski, C., and Baillie, P., 2004. Mesozoic evolution of the Greater Taranaki Basin and implications for petroleum prospectivity. *The APPEA Journal*, *44*(1), 385–396.

Uruski, C., Baillie, P., and Stagpoole, V., 2003. Development of the Taranaki Basin and comparisons with the Gippsland Basin: implications for deepwater exploration. *The* APPEA Journal, 43(1), 185–196.

Vonk, A. J., Kamp, P. J., and Hendy, A. J., 2002. Outcrop to subcrop correlations of late Miocene-Pliocene strata, eastern Taranaki Peninsula. New Zealand Petroleum Conference proceedings, pp. 234–255.

Weimer, P., and Link, M. H., 1991. *Seismic Facies and Sedimentary Processes of Submarine Fans and Turbidite Systems*. New York, Springer-Verlag, 447 pp.

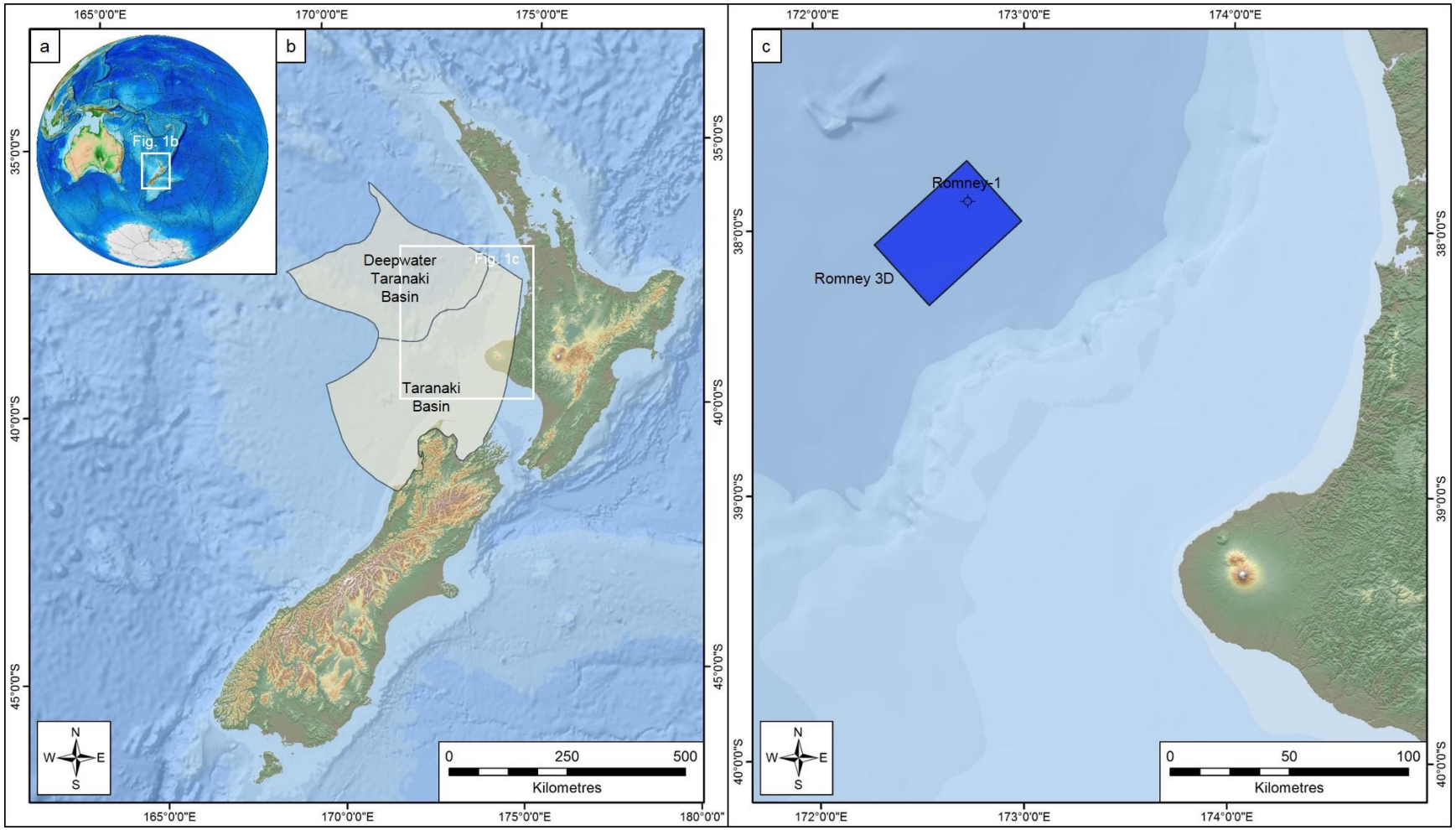

Figure 1. a) Global inset showing the position of New Zealand in the south Pacific. b) Regional New Zealand topographic map shows location of detailed study area presenting the Taranaki Basin and its subdivisions. c) Location of the study area including the Romney 3D seismic survey and the Romney-1 well.

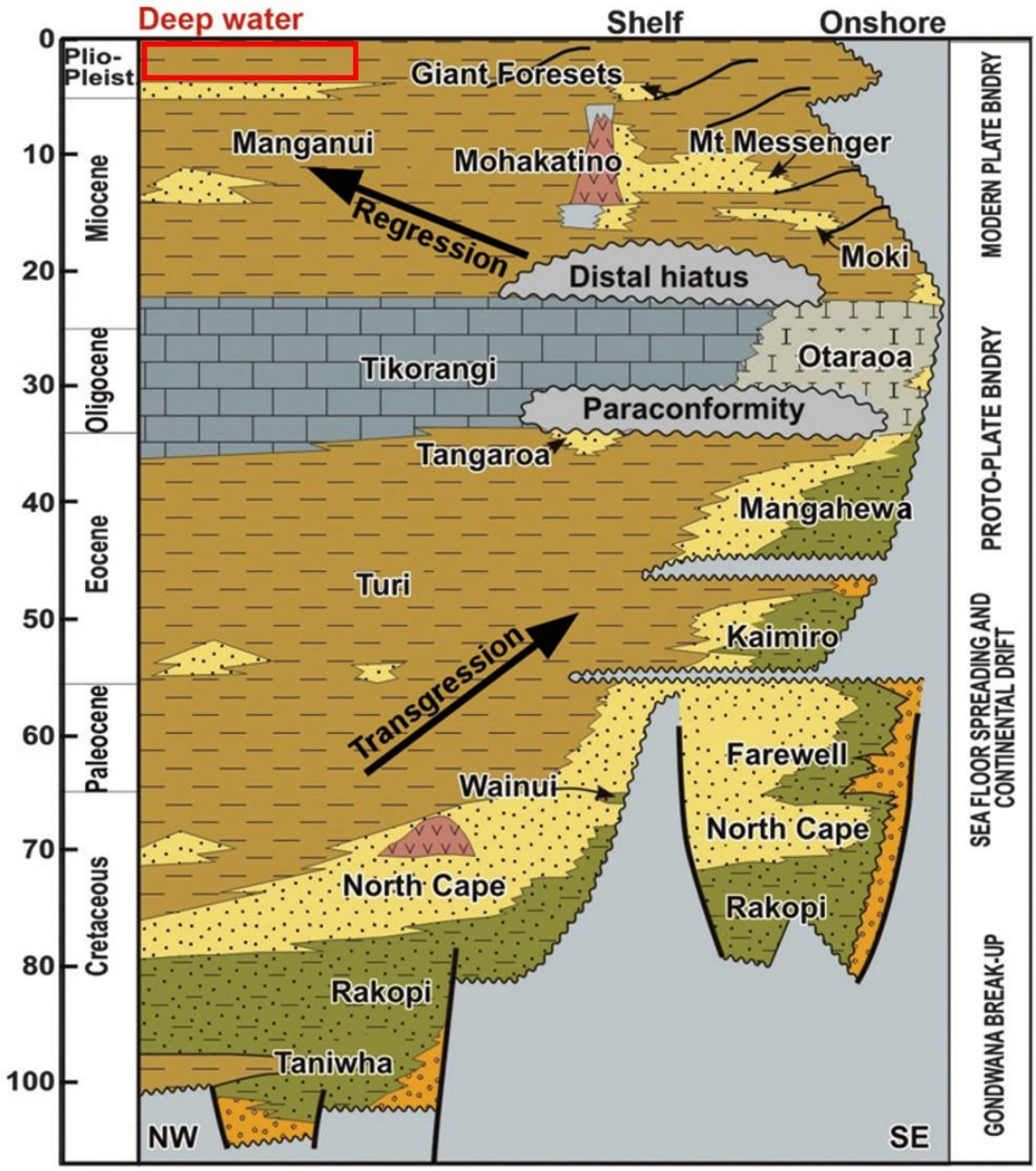

Figure 2. Taranaki basin stratigraphic column. The study interval (red rectangle) belongs to Plio-Pleistocene deposits laterally equivalent to the Giant Foresets Formation on the shelf and onshore. Modified from Baur et al. (2014).

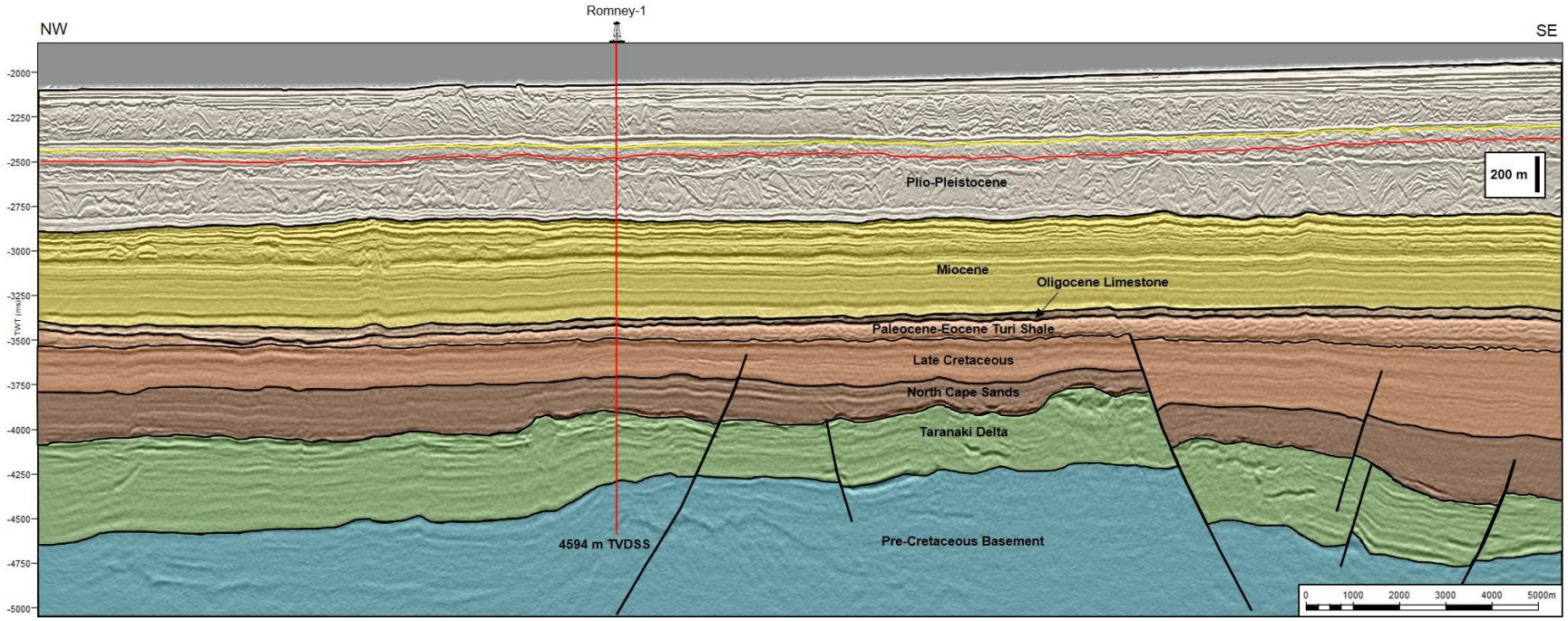

Figure 3. Geoseismic section showing the general stratigraphy and structure of the area of study. Red and yellow horizons are the boundary surfaces of the MTD-D, which is the object of the present work. Metric depth scale is valid for the Plio-Pleistocene interval.

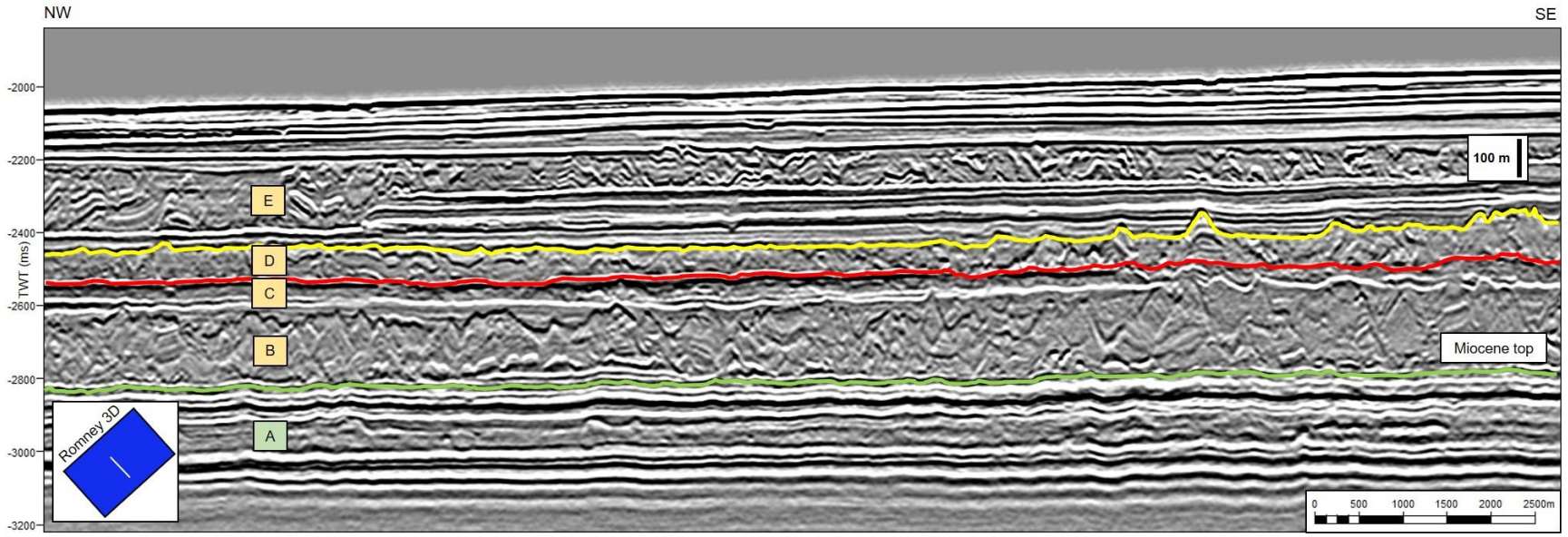

Figure 4. Romney 3D crossline displaying horizons of interest: Miocene top (green), MTD-D base (red), and top (yellow). Other Plio-Pleistocene mass transport deposits (yellow boxes) and one Miocene (green box), showing different thicknesses and and a non-cyclic pattern, have also been identified and named according to the stratigraphic occurrence. Mass transport deposits are separated by horizontal continuous reflectors interpreted as healing phase deposits.

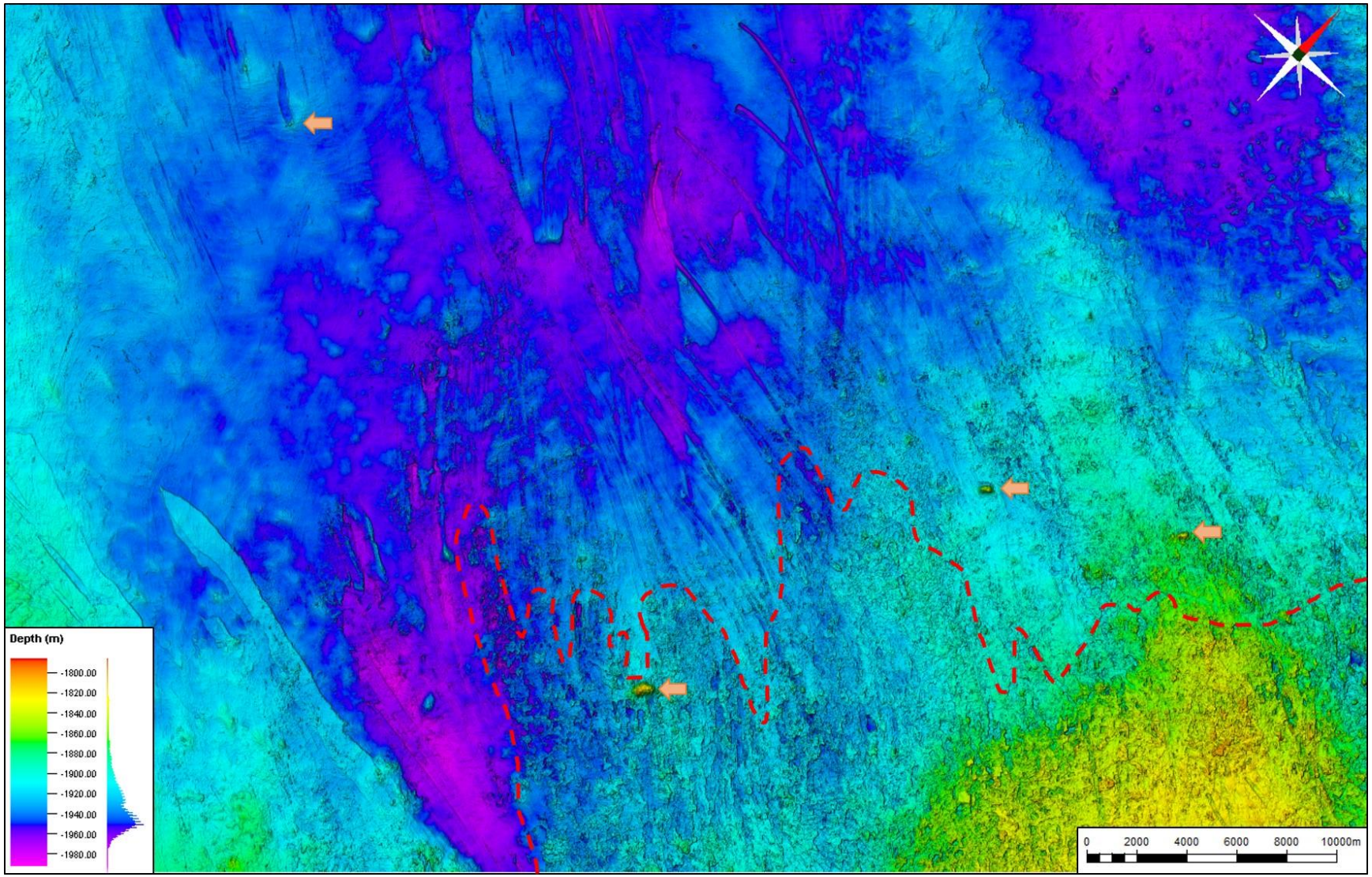

Figure 5. MTD-D basal surface depth map (red horizon on Figures 3 and 4). Red dashed line shows the area of the coalesced base; note a higher relief due to the underlying previous deposit. Orange arrows show the position of protruding blocks deposited by underlying mass transport deposits.

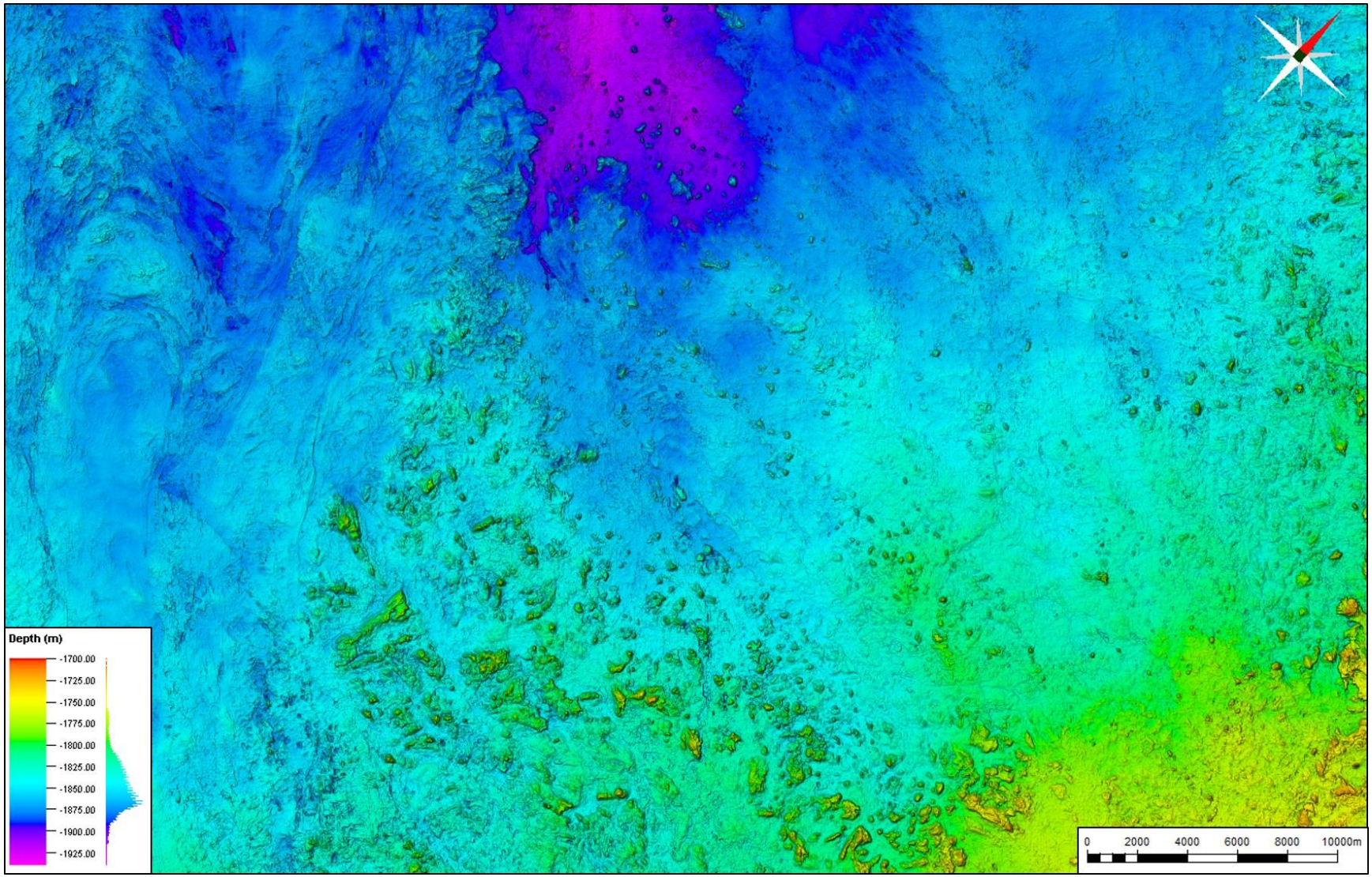

Figure 6. MTD-D top surface in depth (yellow horizon on Figures 3 and 4) exhibits an irregular and blocky relief in the center, pressure ridges in the western corner and isolated scattered blocks in the central northwestern limit of the survey.

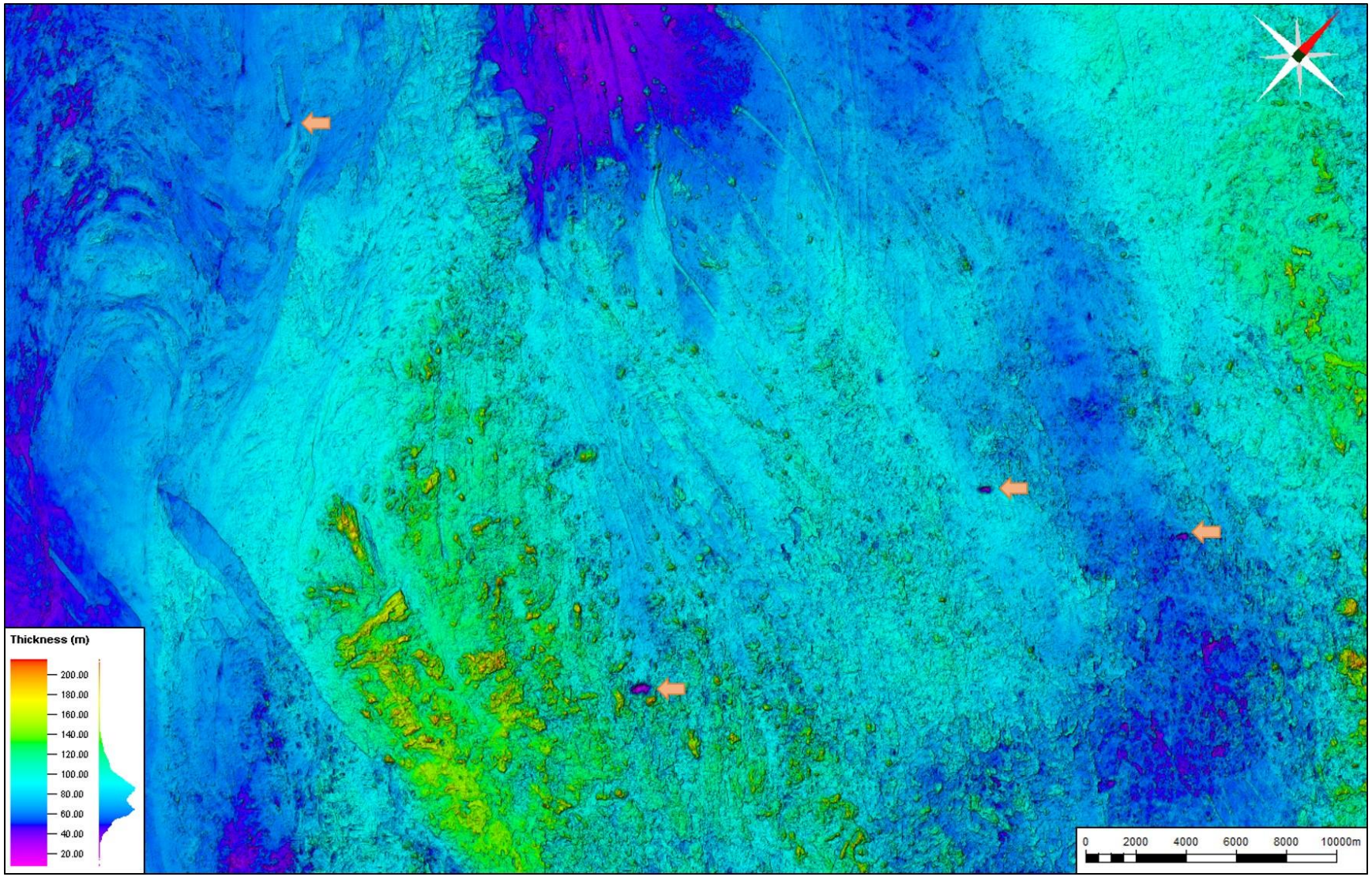

Figure 7. MTD-D isochore, showing true vertical thickness. Orange arrows show a significantly thinner expression of the interval in the position of the protruding blocks deposited by previous mass transport deposits.

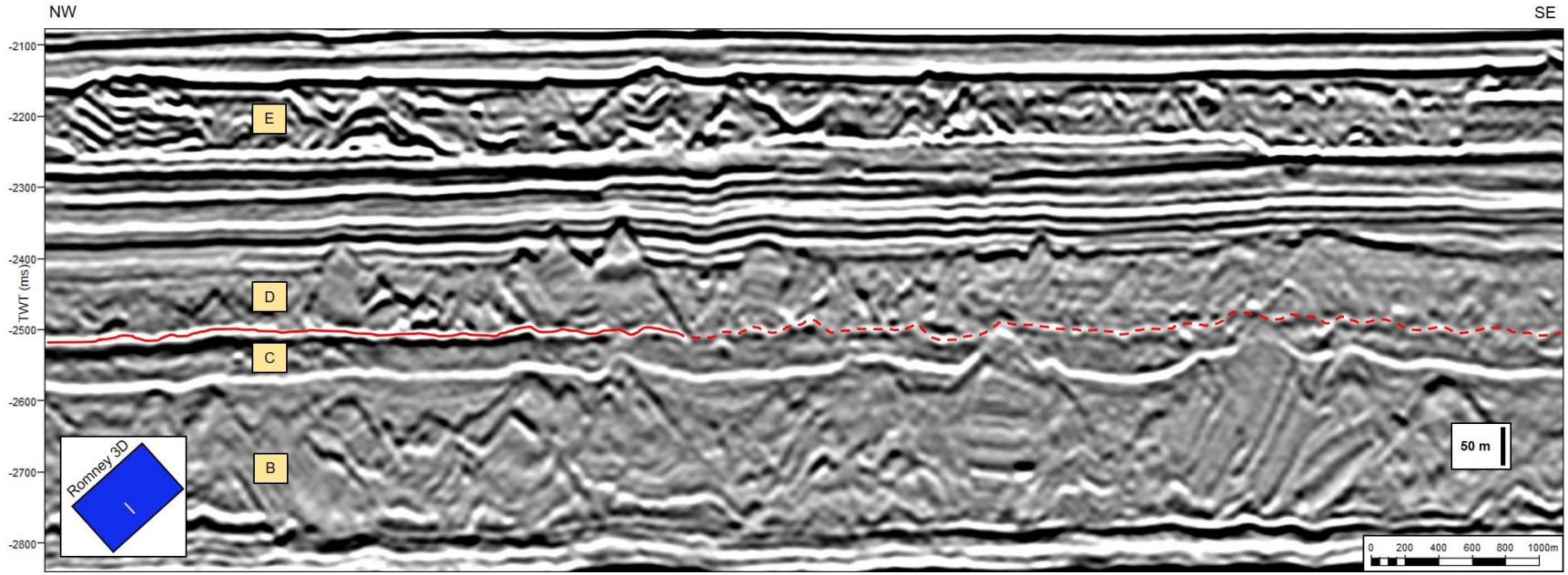

Figure 8. Seismic profile showing the MTD-D basal surface (red horizon). The basal negative reflector has higher amplitude and continuity basinward (NW direction), covering the high positive amplitude drape. Toward proximal areas (SE), the reflector is less continuous and lower in amplitude, due to the absence of the condensed-section drape and consequent coalescence with the underlying MTD-C.

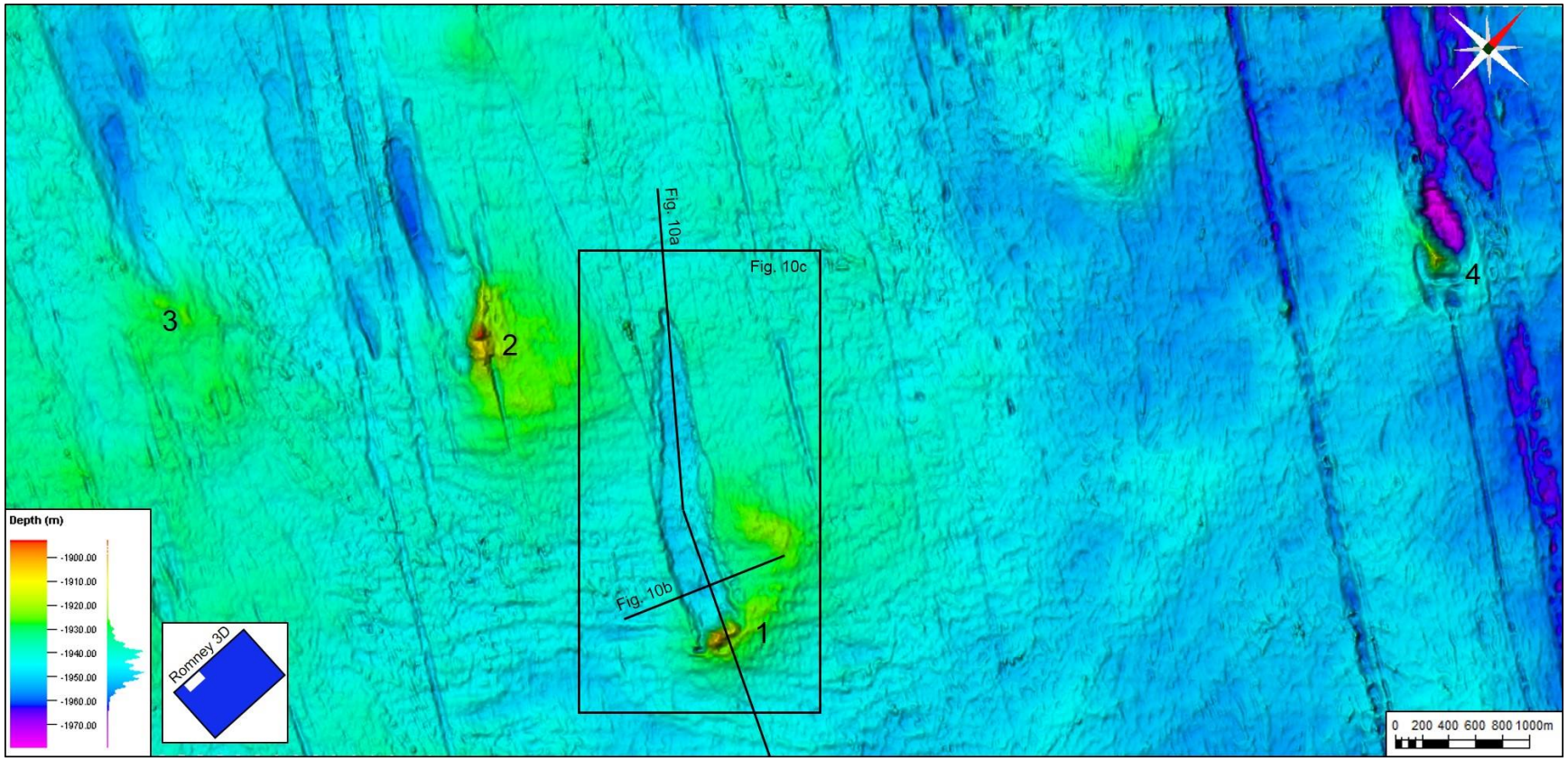

Figure 9. Shield blocks area basal surface. Blocks are enumerated (1-4) and number 1 is interpreted in further figures. Note bathymetric lows downslope (W-NW) the blocks, named “erosional shadow scours” in the present work.

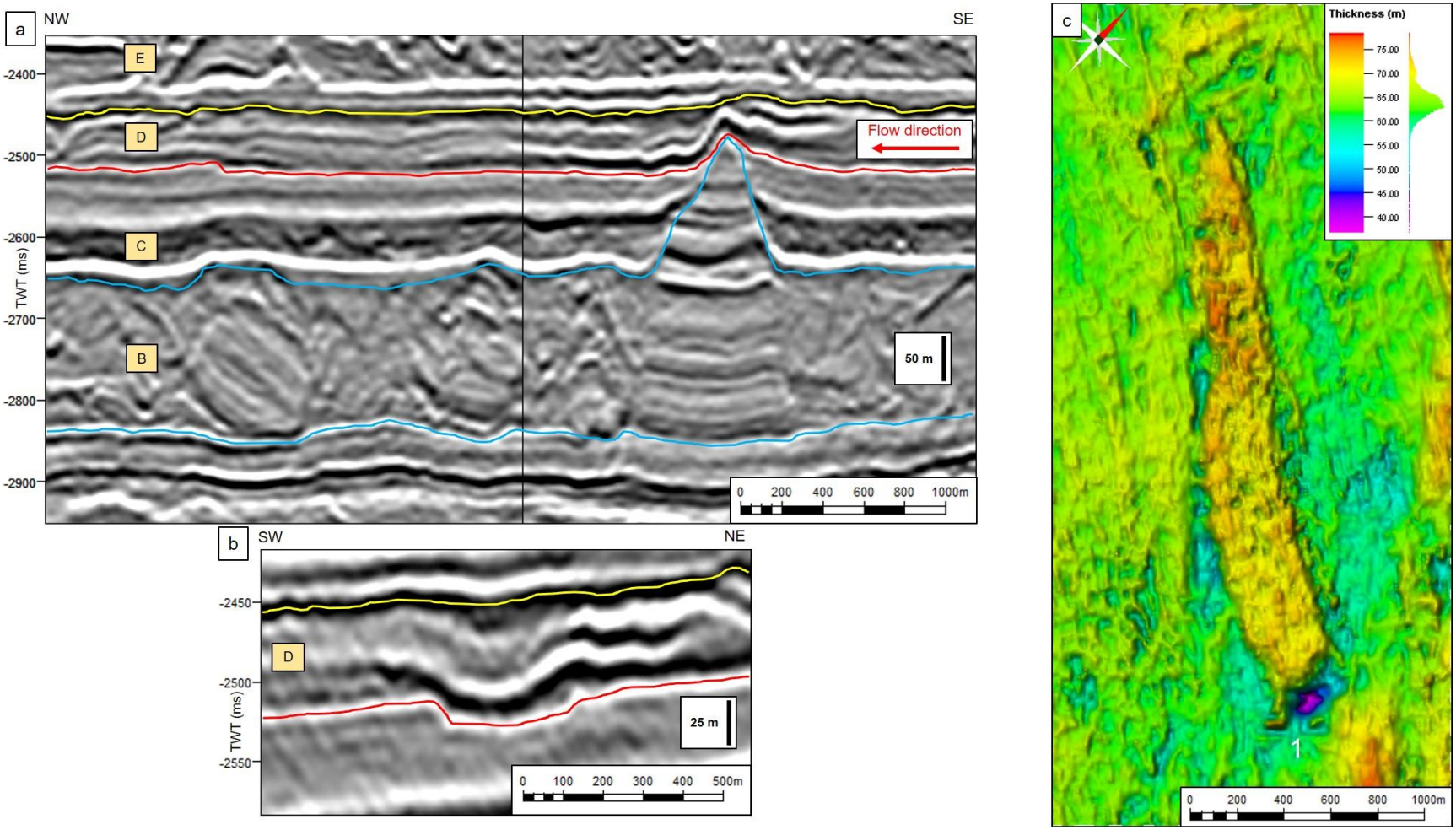

Figure 10. a) Longitudinal cross section shows the internal view of the deposit denoting the origin of the shield block and the relationship with the overlying deposits (location in Figure 9). The shield block was deposited within the MTD-B, bounded by blue horizons, partially covered by healing phases and ultimately capped by MTD-D, defined by the red and yellow horizons. The basal red horizon depicts a 2.5 km long and 30 m deep erosional shadow scour down system (NW) the shield block that is later covered by the mass transport deposit. b) The relief is also seen in transversal view, where the width is approximately 400 m (location in Figure 9). c) True vertical thickness map (location in Figure 9). Observe a thinner expression above the shield block and a thicker one basinward covering the erosional shadow scour (NW), compared to the surrounding areas.

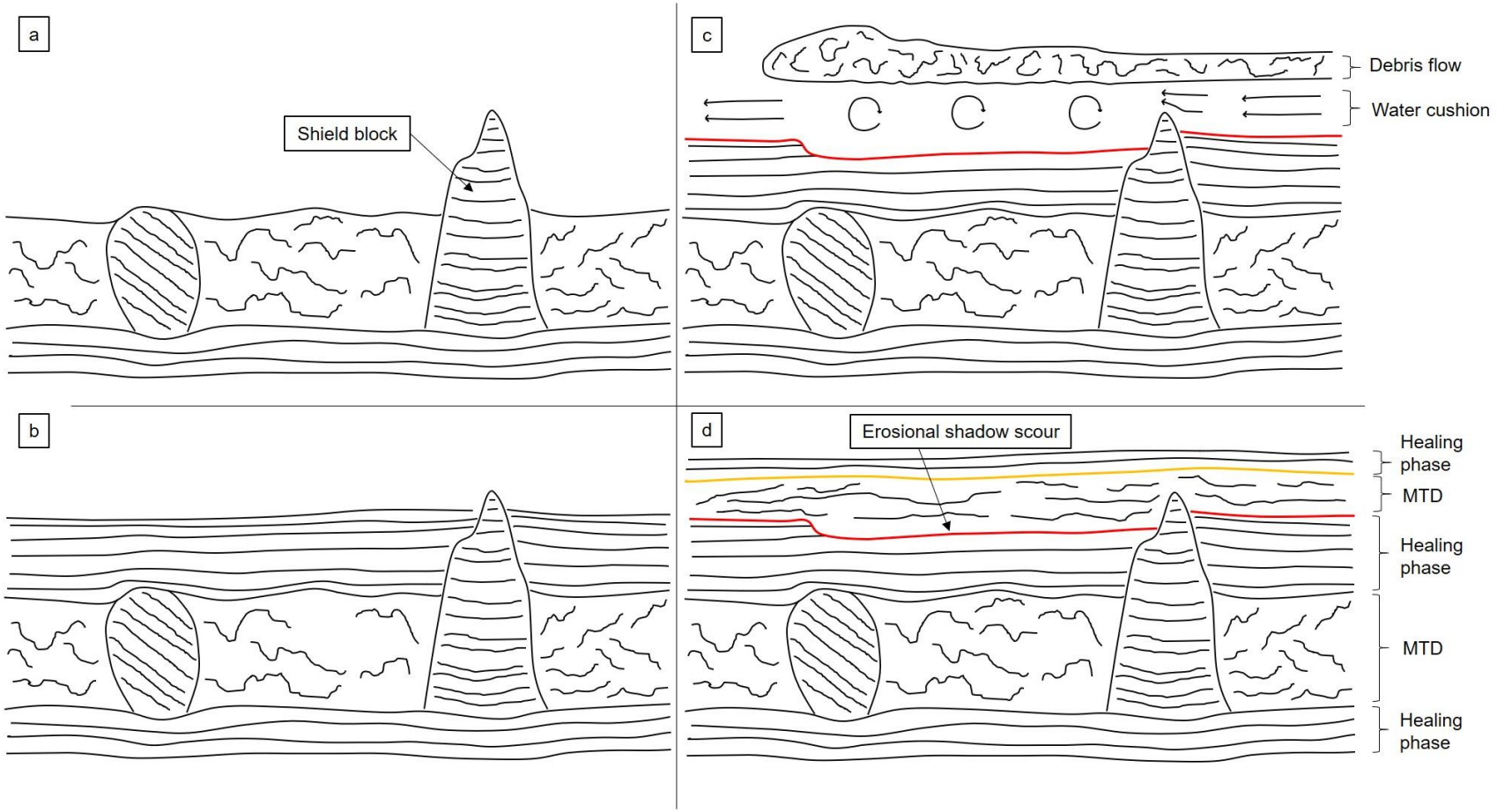

Figure 11. Schematic explanation of the development of ESSs. a) A mass transport deposit bearing large blocks is deposited over the preexistent seafloor. b) Healing phase deposits (mudflows and turbidites) level the irregularities and partially cover the protruding block. c) The laminar flow (straight lines) of the hydroplaning water cushion corresponding to a subsequent MTD hits the obstacle and develops a local turbulence (rounded arrows) down flow that erodes the seafloor developing an elongate scour, while the debris flow runs above it. After a certain distance, the turbulence is attenuated, and the flow recovers its laminar state. d) The flow deposits its sediment charge which fills the negative feature (erosional shadow scour) and is ultimately capped by new healing phase deposits.

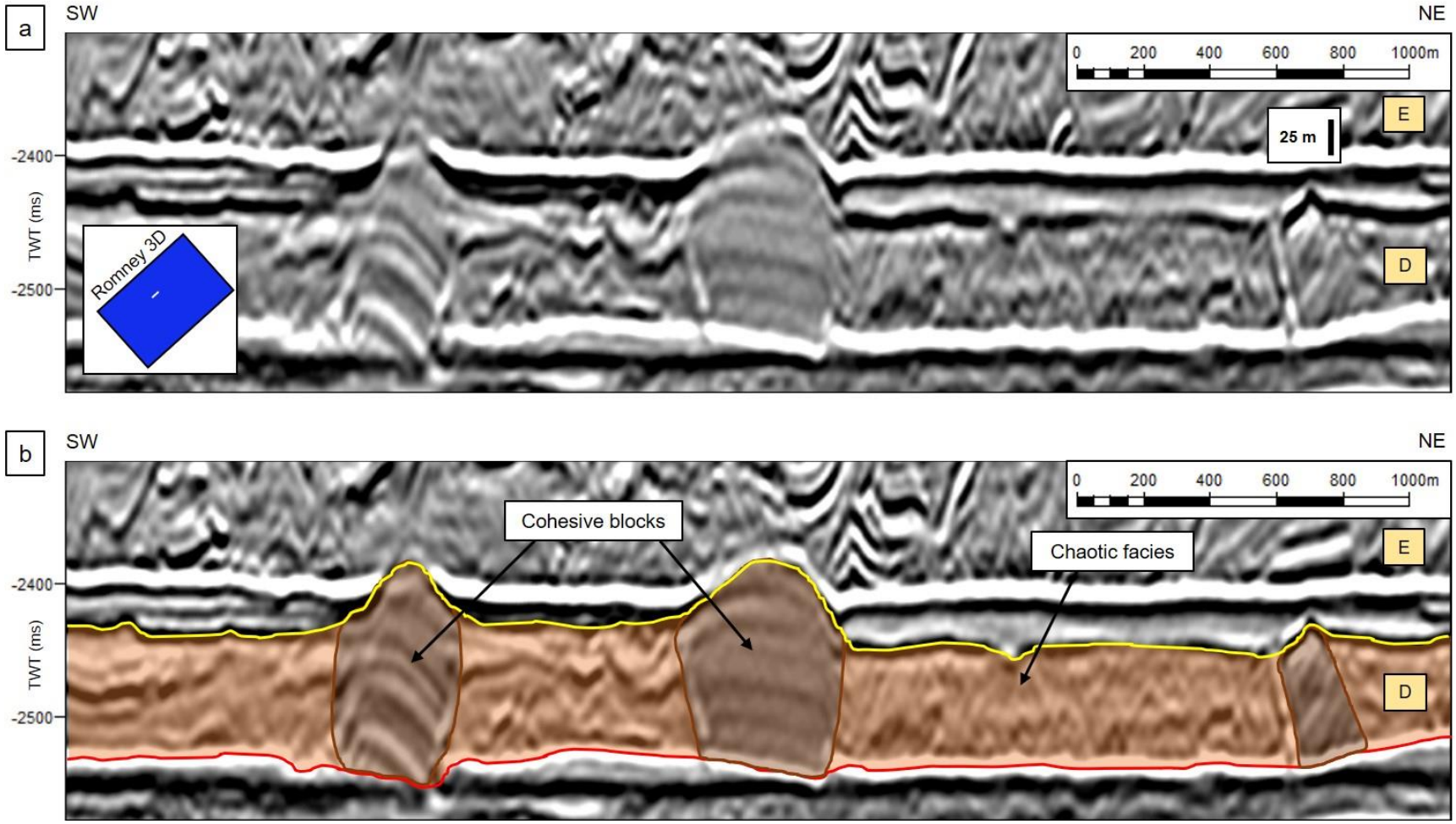

Figure 12. a) Clean seismic profile portraying the internal body of the MTD-D. b) Interpreted seismic profile showing coherent packages of seismic facies (brown) among chaotic, semi-transparent, low impedance reflection patterns (orange), interpreted as cohesive remnants of the failed paleo slope from where MTD-D was originated, within a disaggregated matrix.

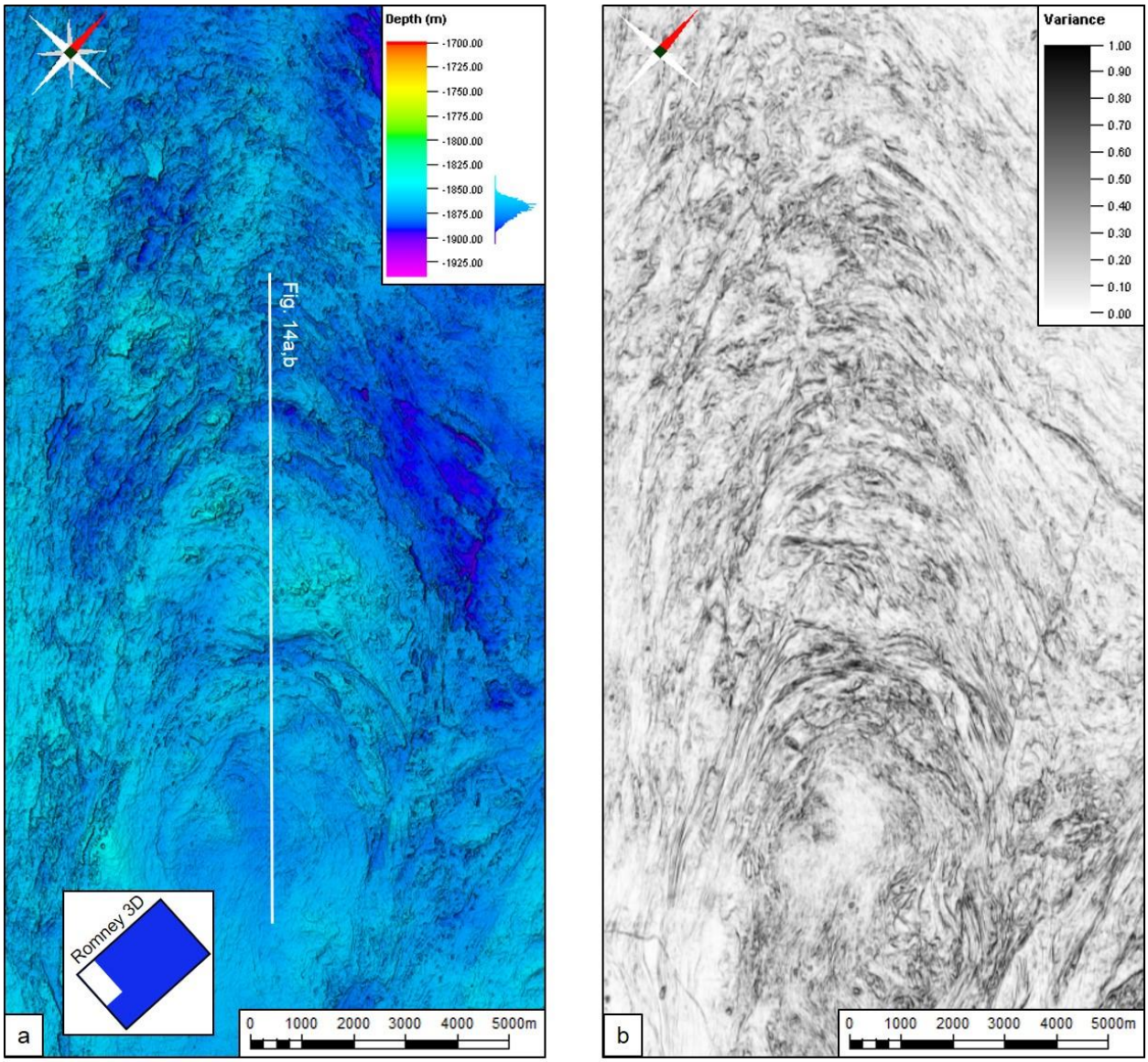

Figure 13. View of the pressure ridges area. a) Depth structure map of the MTD-D top surface. Note a higher relief and more preserved shape of the pressure ridges in proximal areas than in distal ones. b) Variance time slice at -2464 ms two-way time, showing the feature's internal structure. The flanks of the ridges present higher variance values than the center, which provides evidence of discontinuity between one ridge and the immediate next.

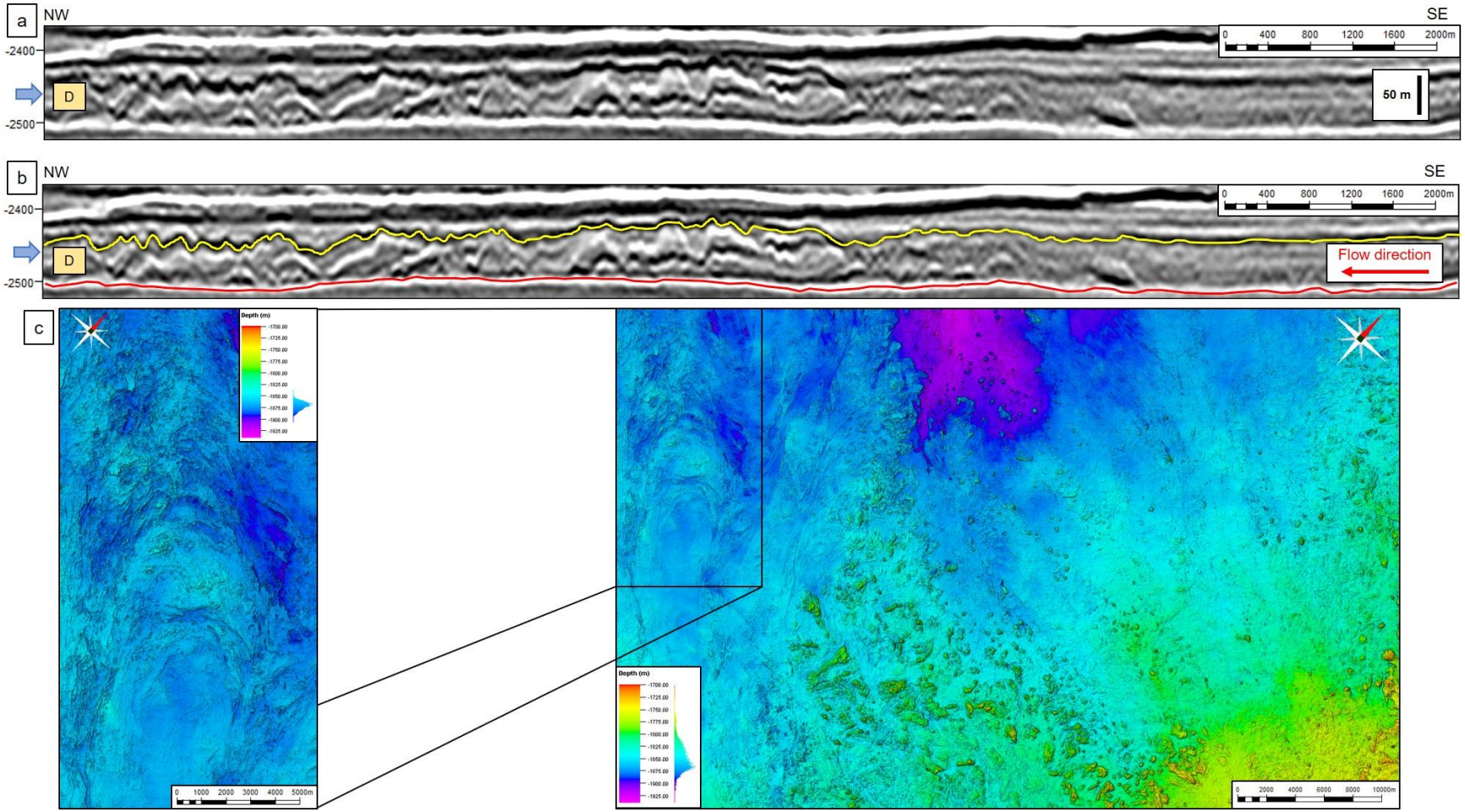

Figure 14. a) Cross section seismic profile of the pressure ridges (NW) and the undisturbed top surface (SE) (location in Figure 13a). Blue arrow shows the position of the variance time slice (-2464 ms) in Figure 13b. b) Interpreted cross section seismic profile. Rugged yellow surface toward the NW represents the relief developed by the pressure ridges. Blue arrow shows the position of the variance time slice (-2464 ms) in Figure 13b. c) MTD-D top surface (yellow horizon in Figure 14b) and detail to the pressure ridges area.

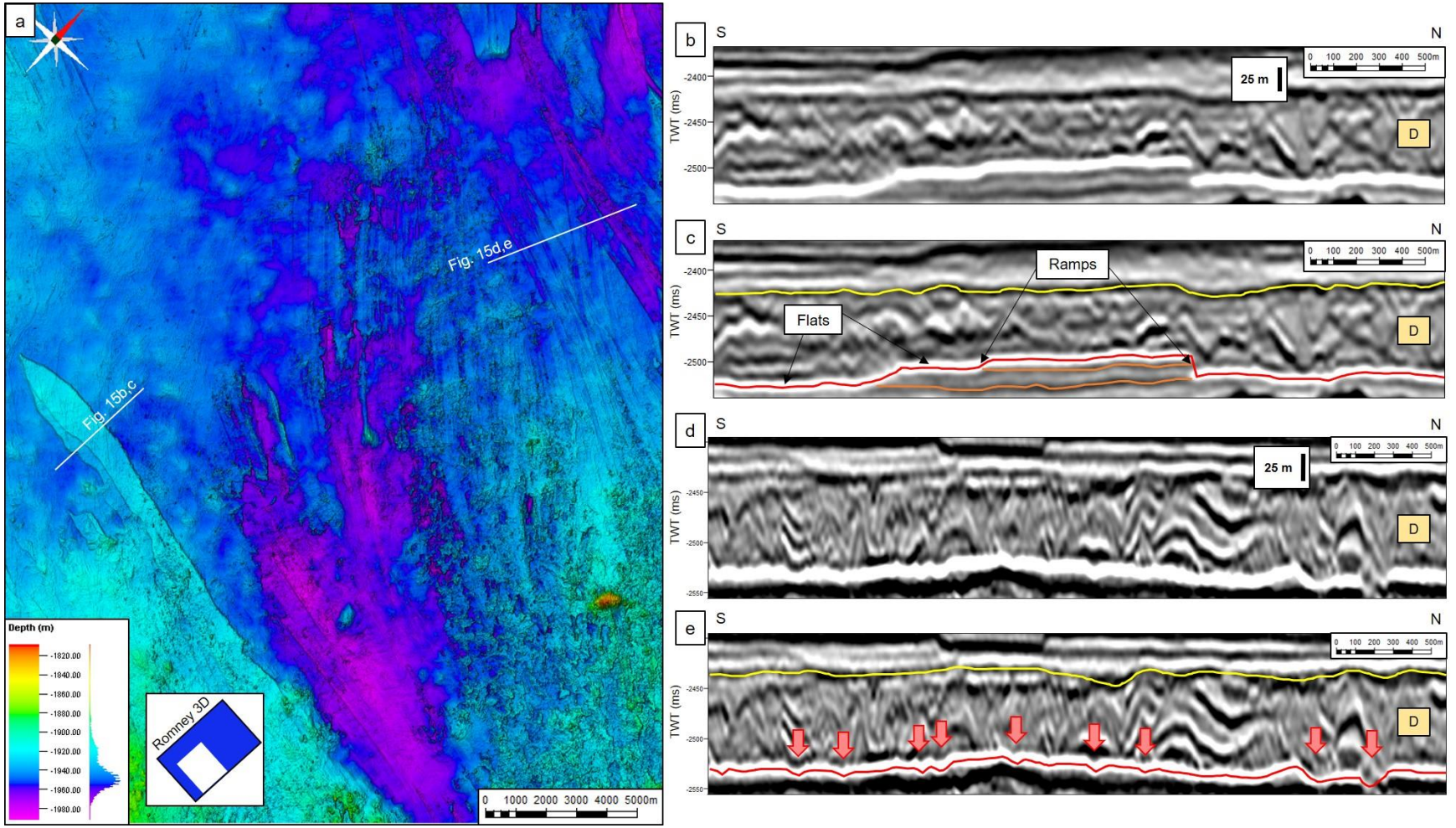

Figure 15. a) Close up of the MTD-D basal surface (red horizon in Figures 15c, e) showing ramps and flats, and grooves. Observe the divergent character of some grooves from the SE margin toward the center of the map, which are interpreted as "monkey fingers". b) Ramps and flats in cross section seismic profile (location in Figure 15a). c) Interpreted ramps and flats cross section seismic profile. Note that the underlying parallel horizons (orange) are cut at different stratigraphic levels, connected by the ramps. d) Grooves cross section seismic profile (location in Figure 15a). e) Interpreted grooves cross section seismic profile. Red arrows indicate the typically "v"-shaped striations.

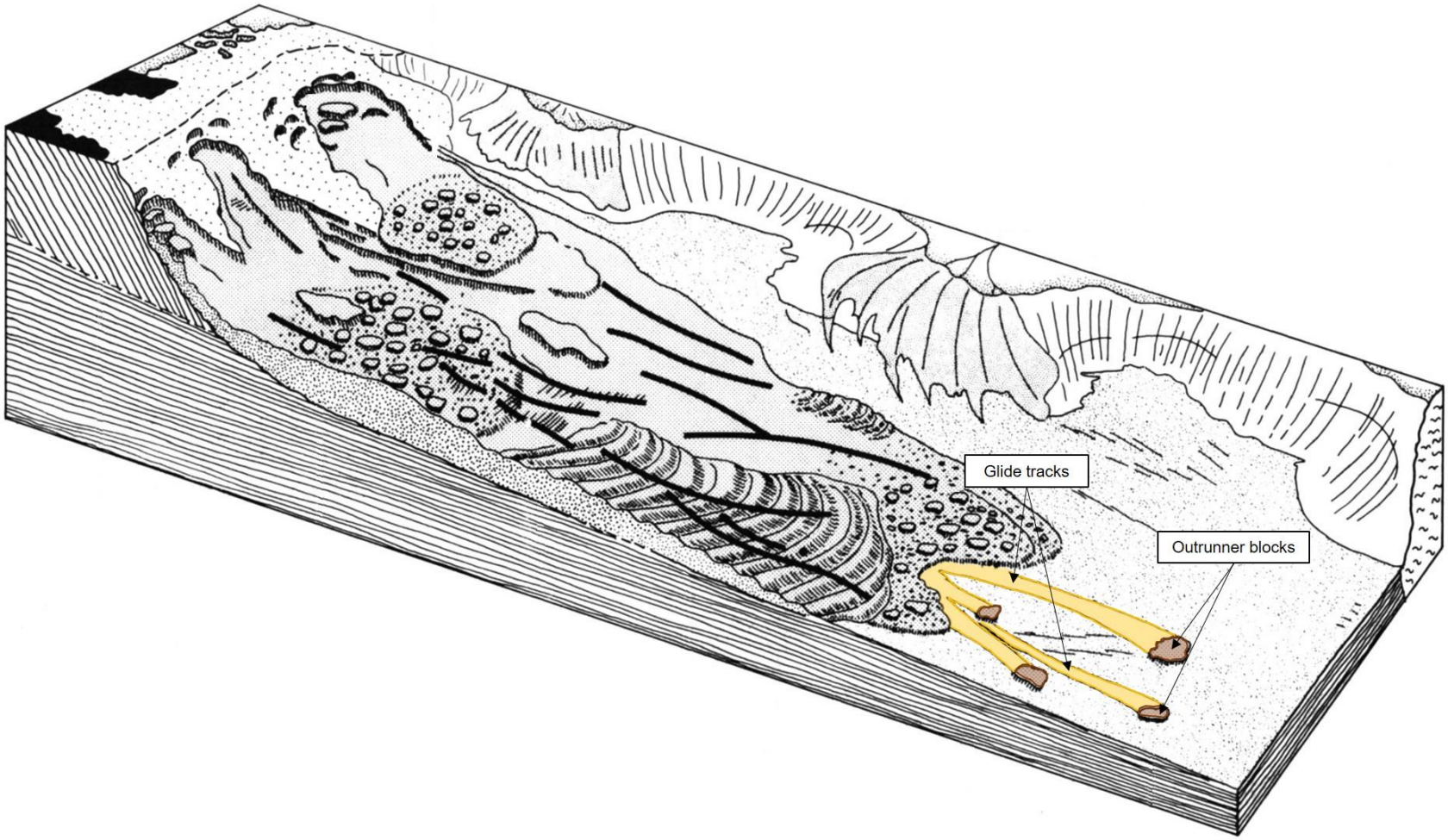

Figure 16. Position and characteristics of the glide tracks and outrunner blocks. The objects individually detach from the flow front and run freely downslope, each leaving its own scour. Modified from Prior et al. (1984).

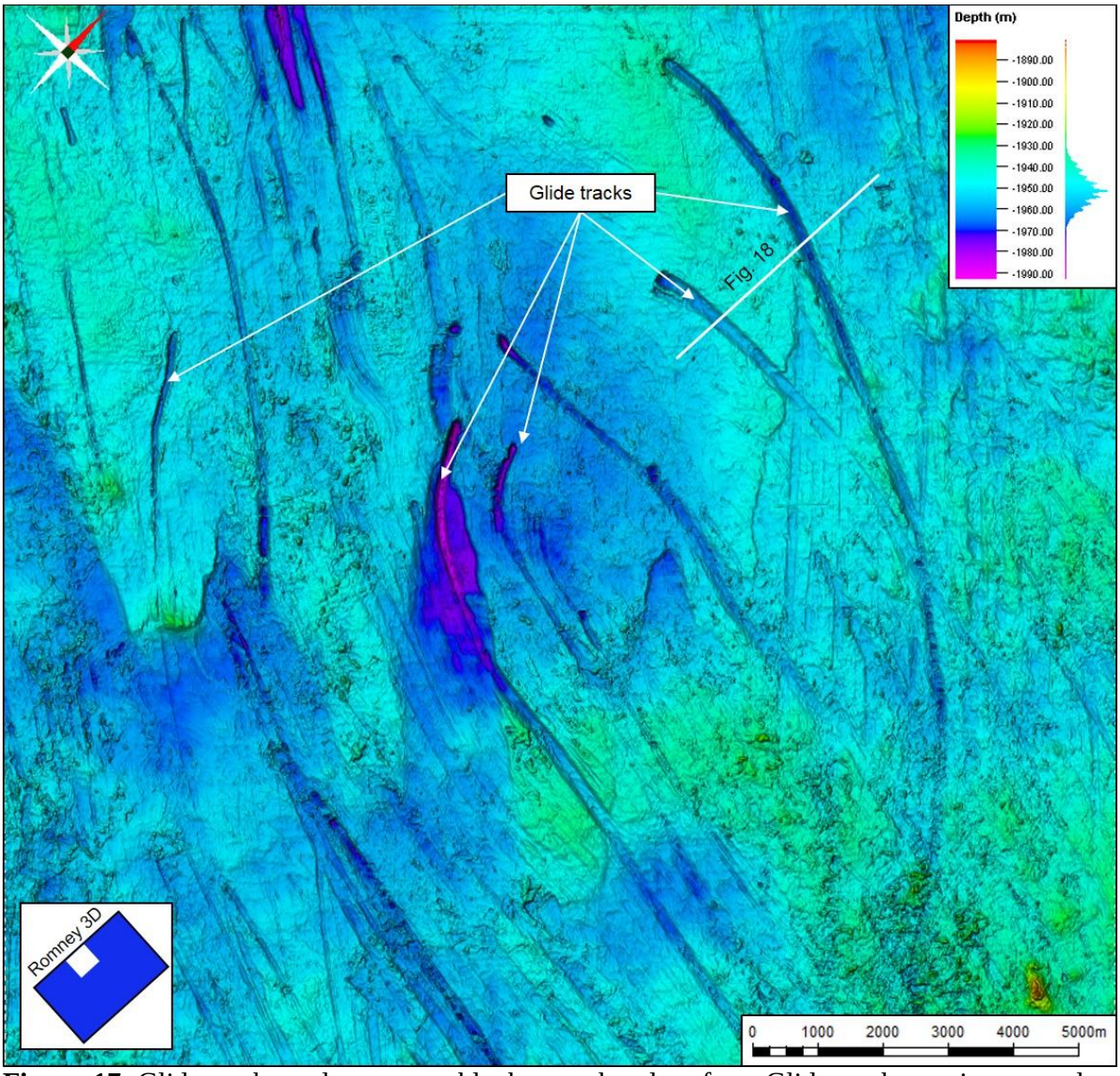

Figure 17. Glide tracks and outrunner blocks area basal surface. Glide tracks are interpreted as elongate individual lineal erosional features, sometimes slightly to moderately curved developed by the gouging of outrunner blocks that run freely downslope detached from the main flow.

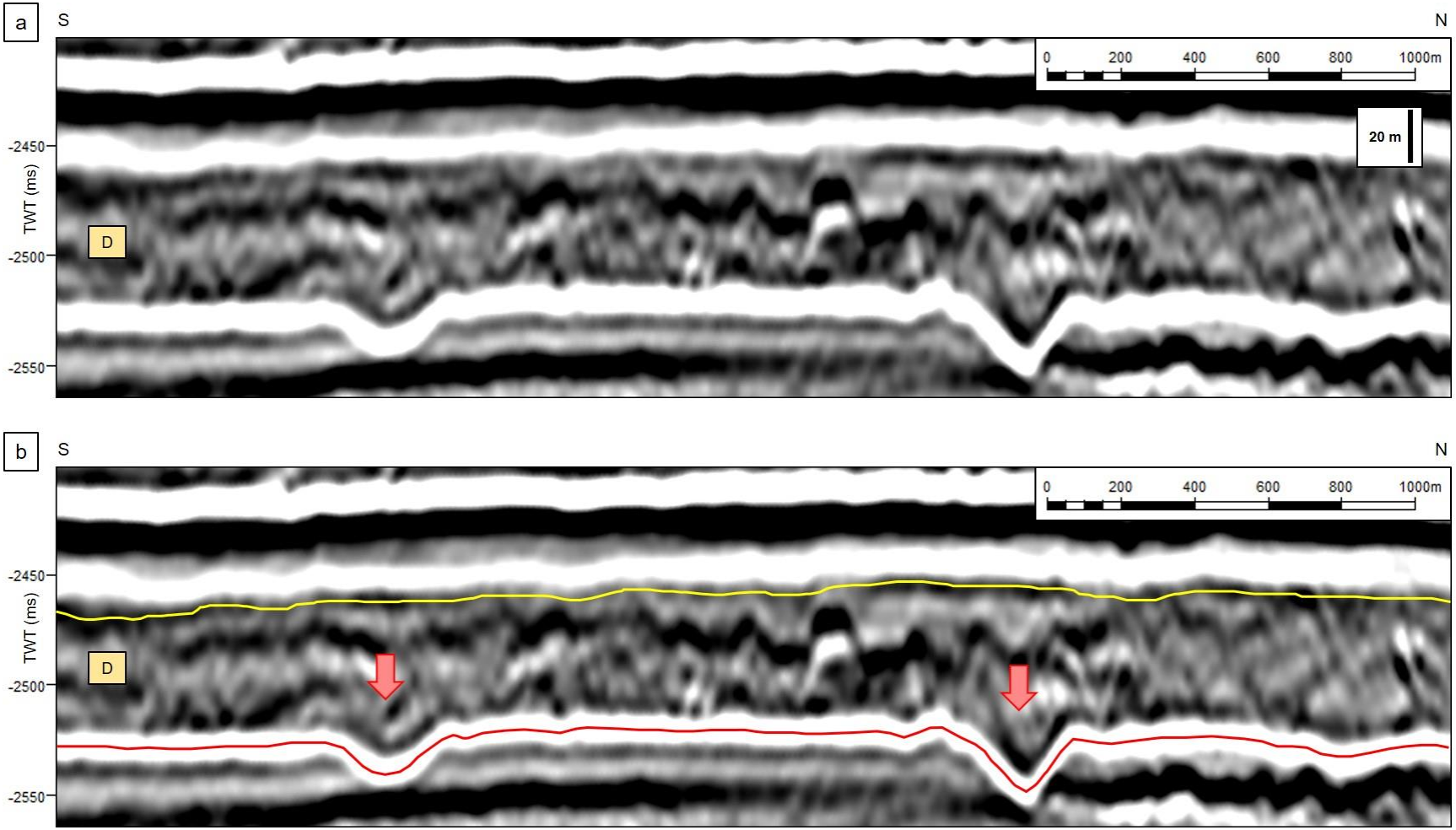

Figure 18. a) Clean transversal cross section seismic profile showing the geometry of the glide tracks (location in Figure 17). b) Interpreted transversal cross section seismic profile showing the geometry of the glide tracks (red arrows). Note the differences in the shape of the tracks: the southern one exhibits a nearly flat base whereas the northern presents a sharper one.

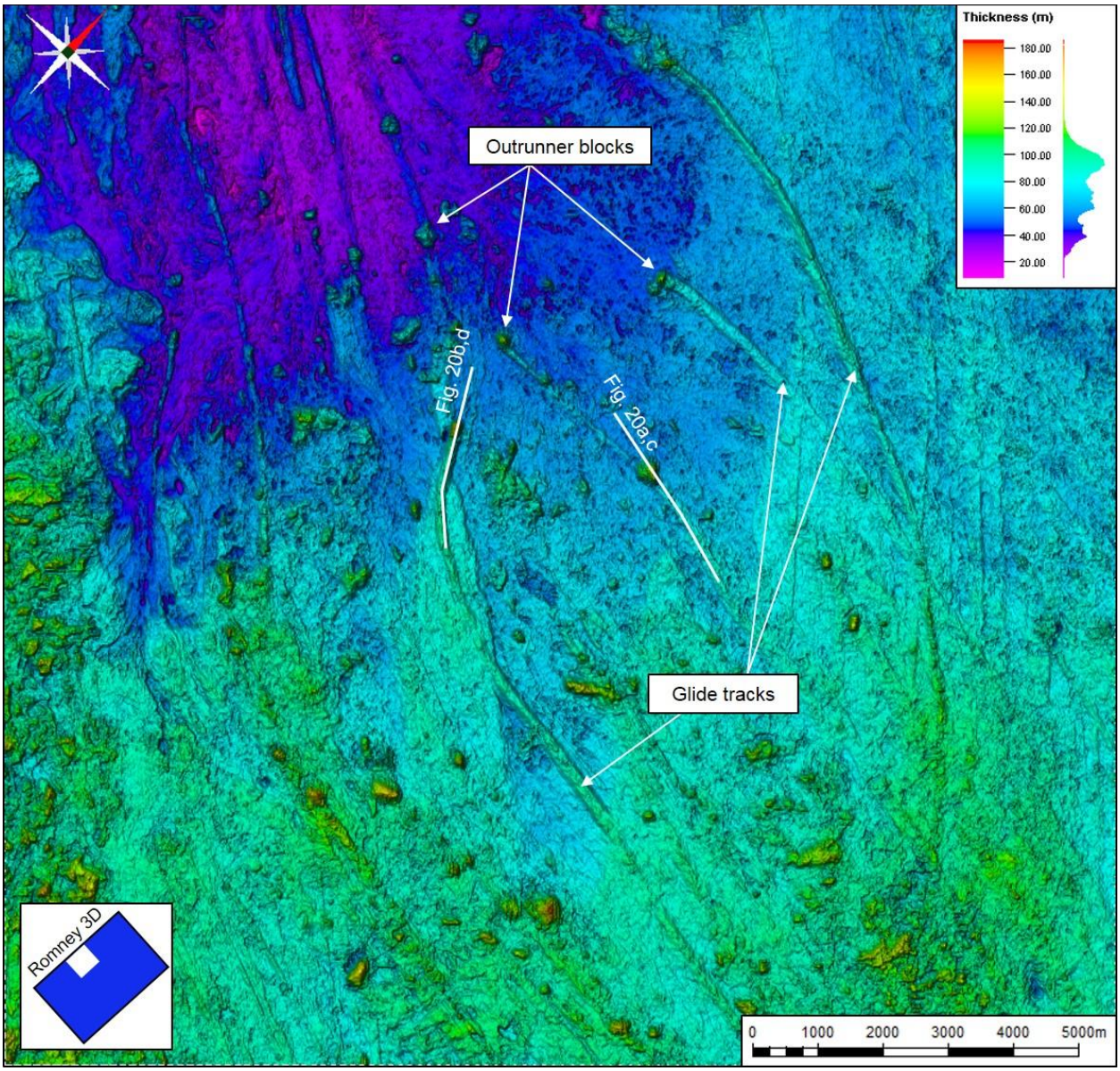

Figure 19. True vertical thickness map of the glide tracks and outrunner blocks area. The glide tracks exhibit a thicker expression than the immediate surrounding deposits and usually preserve, at their end, the corresponding outrunner block.

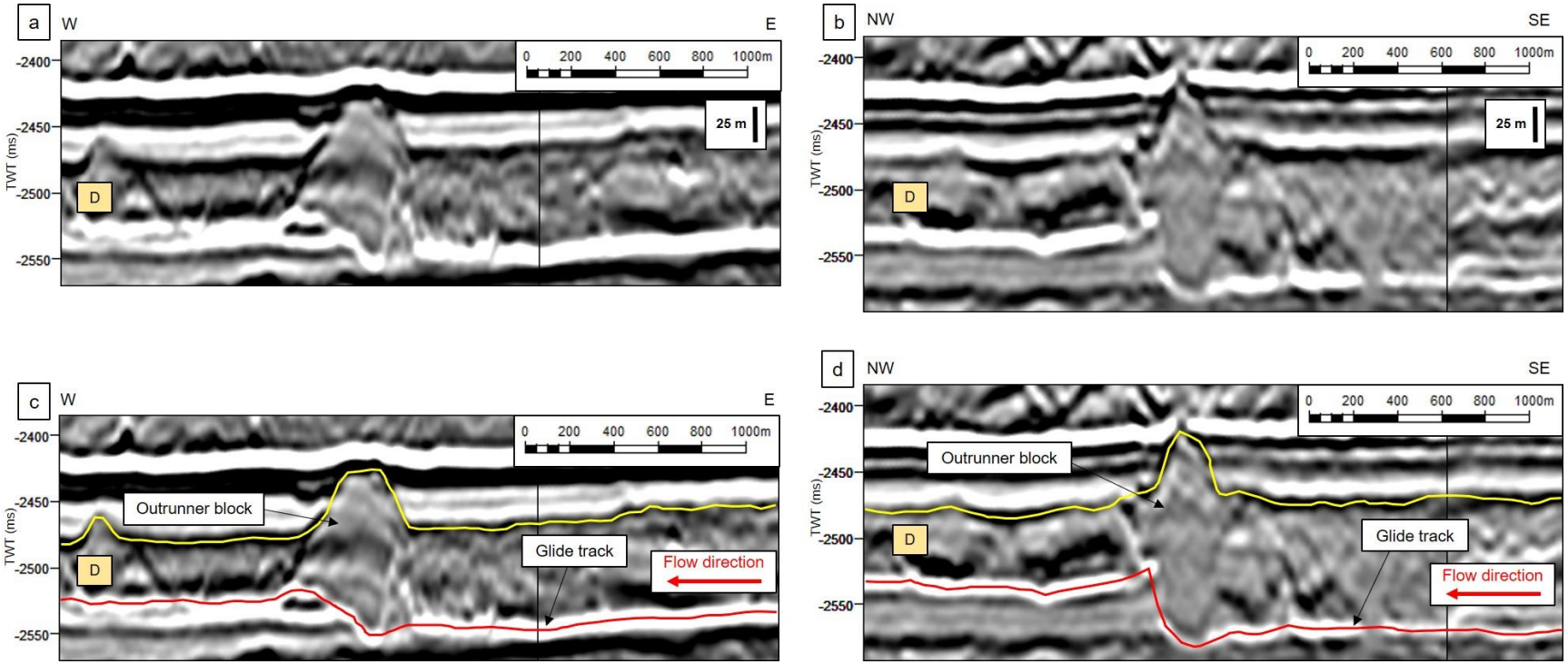

Figure 20. a), b) Clean longitudinal cross section seismic profiles showing the geometry of the glide tracks (location in Figure 18). c), d) Interpreted transversal cross section seismic profiles display the preserved outrunner blocks at the end of the glide tracks. Note the thicker expression of the deposit that fills the glide track compared to the undisturbed paleo-seafloor in front of the block.

Appendix

Interpretation of the features herein named "erosional shadow scours" may arise the question of whether they might be not a real surface element but a velocity anomaly artifact. This effect would consist of a velocity push-down induced by low velocity material within the "scour" compared to the immediate lateral equivalents outside the feature (Sheriff, 2002). A velocity push-down would generate a travel time delay of the basal MTD-D reflector due to extra travel time through the low velocity area. Figure 21 displays a sketch of the variables for this case.

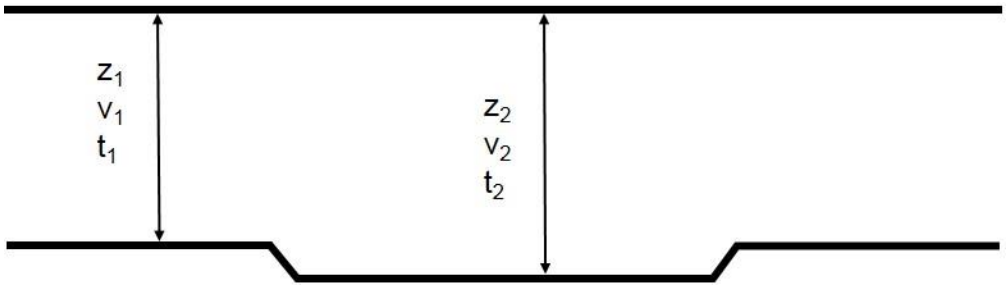

Figure 21. Sketch showing the reflector delay in time and the variables. z_1: MTD-D thickness outside the "scour"; v_1: MTD-D seismic velocity outside the "scour"; t_1: MTD-D two-way time outside the "scour"; z_2: MTD-D thickness inside the "scour"; v_2: MTD-D seismic velocity inside the "scour"; t_2: MTD-D two-way time inside the "scour".

Assuming that the scour does not really exist and that it is only an effect of velocity, the thicknesses both inside and outside the potential scour should be equal ($z_1 = z_2$) and the time delay would be only an effect of lateral velocity variation.

Depth conversion is given by the product of the velocity and the two-way time, divided by two (Liner, 2016):

$$\frac{v_1 t_1}{2} = \frac{v_2 t_2}{2}$$

where v_1 is the velocity of MTD-D in the rest of the survey (1850 m/s). The times t_1 (65.85 ms) and t_2 (75.48 ms) were averaged from MTD-D time-thickness immediately around and inside the scour, respectively. The velocity of the material inside the scour (v_2) is the unknown variable:

$$v_2 = \frac{v_1 t_1}{t_2}$$

$$v_2 = \frac{1850\ \frac{m}{s} \times 65.85\ ms}{75.48\ ms}$$

$$v_2 = 1613.97\ \frac{m}{s}$$

This analysis provides an estimate of 1614 m/s as the velocity required to develop the observed time delay. There are three lines of evidence suggesting the scour feature is due to structural thickening and not lateral velocity variation.

First, a velocity of 1614 m/s for a Plio-Pleistocene consolidated material, considering that the water velocity in the survey is 1500 m/s, seems to be unrealistic.

Second, a lateral velocity should develop a time sag depressing all deeper structure (Herron, 2011), an effect not observed in our data. Figure 22 shows a cross section demonstrating evidence that only the basal MTD-D event shows the scour structure.

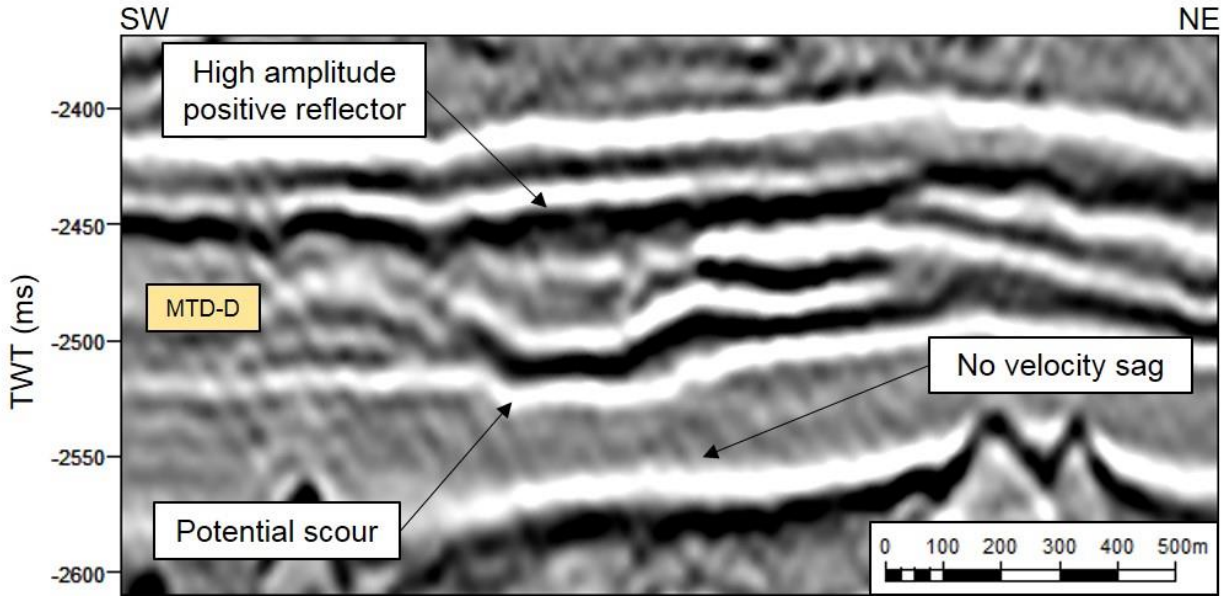

Figure 22. Cross section seismic profile of the "scour" under study. No velocity sag is evidenced below the structure: if this would happen, the white reflector below the "scour" should also be experiencing a push-down. Good examples of real cases are shown in Herron (2011). The top boundary right above the deposit within the "scour" is seen as a high amplitude positive reflector

(black). If the scour was a velocity effect, this reflector should be a high amplitude negative reflector (white).

Third, a lateral velocity change would result in an impedance change leading to lateral variation in the reflection amplitude of the MTD-D top reflector. Specifically, a drop in velocity sufficient to explain the basal time sag would lead to a strongly negative reflector amplitude over the scour area, which is not observed in the data (Figures 22, 23).

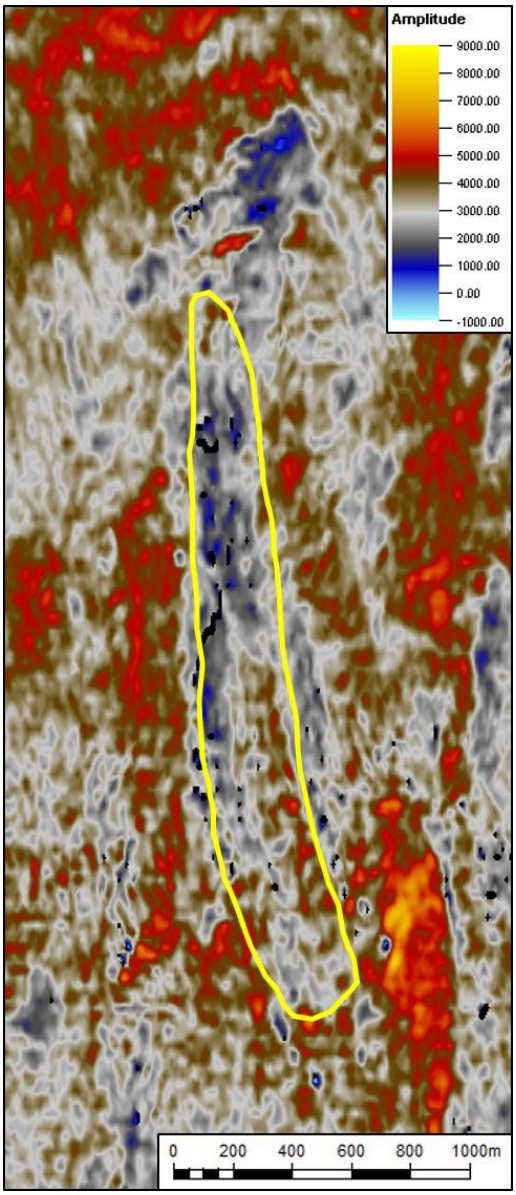

Figure 23. Amplitude local map for MTD-D top horizon. A yellow outline shows the position of the "scour". Amplitude values are entirely positive throughout the area, and no evident changes are detected within the scour.

In summary, there are at least three reasons why the velocity anomaly artifact explanation is highly unlikely: an unrealistic velocity value, absence of velocity sag in deeper zones and inconsistency in the expected reflection coefficients. Therefore, the observed scour feature cannot be due to lateral velocity variation and is treated herein as a real negative erosive feature.